



## Opening Pandora's box: reducing global circulation model uncertainty in Australian simulations of the carbon cycle

Lina Teckentrup<sup>1,2</sup>, Martin G. De Kauwe<sup>3</sup>, Gab Abramowitz<sup>1,2</sup>, Andrew J. Pitman<sup>1,2</sup>,  
Anna M. Ukkola<sup>1,2</sup>, Sanaa Hobeichi<sup>1,2</sup>, Bastien François<sup>4</sup>, and Benjamin Smith<sup>5,6</sup>

<sup>1</sup>ARC Centre of Excellence for Climate Extremes, Sydney, NSW, Australia

<sup>2</sup>Climate Change Research Centre, University of New South Wales, Sydney, NSW, Australia

<sup>3</sup>School of Biological Sciences, University of Bristol, Bristol, UK

<sup>4</sup>Laboratoire des Sciences du Climat et l'Environnement (LSCE-IPSL) CNRS/CEA/UVSQ,  
UMR8212, Université Paris-Saclay, Gif-sur-Yvette, France

<sup>5</sup>Hawkesbury Institute for the Environment, Western Sydney University, Penrith, NSW, Australia

<sup>6</sup>Department of Physical Geography and Ecosystem Science, Lund University, Lund, Sweden

**Correspondence:** Lina Teckentrup (l.teckentrup@westernsydney.edu.au)

Received: 11 July 2022 – Discussion started: 18 July 2022

Revised: 4 April 2023 – Accepted: 5 April 2023 – Published: 5 May 2023

**Abstract.** Climate projections from global circulation models (GCMs), part of the Coupled Model Intercomparison Project 6 (CMIP6), are often employed to study the impact of future climate on ecosystems. However, especially at regional scales, climate projections display large biases in key forcing variables such as temperature and precipitation. These biases have been identified as a major source of uncertainty in carbon cycle projections, hampering predictive capacity. In this study, we open the proverbial Pandora's box and peer under the lid of strategies to tackle climate model ensemble uncertainty. We employ a dynamic global vegetation model (LPJ-GUESS) and force it with raw output from CMIP6 to assess the uncertainty associated with the choice of climate forcing. We then test different methods to either bias-correct or calculate ensemble averages over the original forcing data to reduce the climate-driven uncertainty in the regional projection of the Australian carbon cycle. We find that all bias correction methods reduce the bias of continental averages of steady-state carbon variables. Bias correction can improve model carbon outputs, but carbon pools are insensitive to the type of bias correction method applied for both individual GCMs and the arithmetic ensemble average across all corrected models. None of the bias correction methods consistently improve the change in simulated carbon over time compared to the target dataset, highlighting the need to account for temporal properties in correction or ensemble-averaging methods. Multivariate bias correction methods tend to reduce the uncertainty more than univariate approaches, although the overall magnitude is similar. Even after correcting the bias in the meteorological forcing dataset, the simulated vegetation distribution presents different patterns when different GCMs are used to drive LPJ-GUESS. Additionally, we found that both the weighted ensemble-averaging and random forest approach reduce the bias in total ecosystem carbon to almost zero, clearly outperforming the arithmetic ensemble-averaging method. The random forest approach also produces the results closest to the target dataset for the change in the total carbon pool, seasonal carbon fluxes, emphasizing that machine learning approaches are promising tools for future studies. This highlights that, where possible, an arithmetic ensemble average should be avoided. However, potential target datasets that would facilitate the application of machine learning approaches, i.e., that cover both the spatial and temporal domain required to derive a robust informed ensemble average, are sparse for ecosystem variables.

## 1 Introduction

Global circulation models (GCMs) are useful projection tools of future climate at continental and global scales but inevitably simulate large biases in temperature, precipitation, and humidity at regional scales and at individual grid points (Randall et al., 2007; Flato et al., 2013). Projections of atmospheric variables from GCMs, represented by the Coupled Model Intercomparison Project (CMIP), underpin a suite of critical future predictions of the carbon and water cycles (e.g., Ahlström et al., 2012; Ukkola et al., 2016; Ahlström et al., 2017), species distributions (Cheaib et al., 2012), species resilience to climate extremes (Sperry et al., 2019), and predictions of conservation planning (Gallagher et al., 2021). Critically, many applications utilize atmospheric variables from GCMs as forcing without explicitly considering underlying uncertainty in their (bias-corrected) climate projections. This uncertainty includes, but is by no means limited to, the fact that CMIP is an “ensemble of opportunity” and not explicitly designed to represent an independent set of estimates; i.e., CMIP models share modules and are related to varying degrees (e.g., Annan and Hargreaves, 2017; Boe, 2018; Abramowitz et al., 2019).

To tackle biases in GCM forcing, a range of approaches have been employed, with no clear agreement or “best practice” on how to assess GCM skill, to bias-correct simulated climate variables, and/or to weight ensemble members. Some studies have quantified the sensitivity of impact studies to GCM selection method, the choice of bias correction, and/or the ensemble-averaging techniques. For example, Gohar et al. (2017) examined the impact of bias correction methods on future warming levels and found that both selecting GCMs based on performance and bias-correcting model data reduced uncertainties in regional projections. In an Australian study, Johnson and Sharma (2015) increased model consensus in future drought projections using bias-corrected simulations. These studies focused either directly on the climate variables and/or derived relatively simple indices based on a single variable. In an analysis of hazard indices based on multiple climate drivers, Zscheischler et al. (2019) showed multivariate methods tended to outperform univariate bias correction methods. In addition, Kolusu et al. (2021) tested the impact of different weighting techniques and two bias correction methods on the spread of hydrological risk profiles and found that the sensitivity to climate model weighting was considerably smaller than the uncertainty resulting from bias correction methodologies. When Ahlström et al. (2012) used CMIP5 simulations to run the dynamic global vegetation model (DGVM) LPJ-GUESS, they found that GCM climate biases translated into a divergence in the future simulated (offline) carbon cycle responses on regional and global scales that was significantly reduced when the climatological input forcing was bias-corrected (Ahlström et al., 2017).

The need to address biases in GCM forcing is commonly acknowledged, but the wide range of possible solutions (e.g., bias correction, ensemble averages across GCMs) makes it difficult to determine the impact of the correction in climate forcing on the specific question of interest. Here, we examine multiple methods to constrain regional projections of the carbon cycle by opening Pandora's box of Greek mythology fame. When Pandora could not resist opening the lid on her box, she allowed all the evils of the world to escape. Similarly, we could not resist testing the impact of various approaches to constraining the carbon cycle, and the challenges we identify are not easily resolvable. However, we hope that by highlighting these challenges we at least begin the process of resolving them.

There have been multiple efforts to constrain future multi-model ensemble uncertainty (e.g., Michelangeli et al., 2009; Knutti et al., 2010b; Bárdossy and Pagram, 2012; Bishop and Abramowitz, 2013; Johnson and Sharma, 2015; François et al., 2020). Most of these attempts assume that the GCMs that simulate the historical climate well are likely to provide more skillful future projections. Based on this assumption, different approaches for dealing with ensemble uncertainty have emerged that can broadly be grouped into three strategies: (i) selecting only a subset of GCMs fit for the respective study (e.g., Pennell and Reichler, 2011; Rowell et al., 2016; Herger et al., 2018; Gershunov et al., 2019), (ii) applying downscaling and bias correction methods (e.g., Panofsky et al., 1958; Wood et al., 2004; Déqué, 2007; Michelangeli et al., 2009; Bárdossy and Pagram, 2012; François et al., 2020), and/or (iii) applying ensemble weighting techniques (e.g., Bishop and Abramowitz, 2013; Sanderson et al., 2017; Massoud et al., 2019, 2020).

The first strategy focuses on sub-selecting GCMs from the full ensemble, using metrics deemed to be application relevant, to obtain an ensemble that is truly representative of the uncertainty linked to GCM simulations. Commonly, this is based on how well GCMs simulate relevant climate variables compared to historical observations (e.g., Kolusu et al., 2021) and represents the “skilled models” category shown in Fig. 1. Other studies find that excluding the “weakest” models has little impact on the overall uncertainty range (e.g., Déqué and Somot, 2010; Knutti et al., 2010b; Rowell et al., 2016). Some studies choose models defined as independent (e.g., based on the correlation of the biases in the simulations or within a Bayesian framework; Jun et al., 2008; Knutti et al., 2010a; Pennell and Reichler, 2011; Annan and Hargreaves, 2017). Lastly, Evans et al. (2014) and Cannon (2015) suggest selecting those models that “span” the (plausible) CMIP projections when selecting GCMs for dynamical downscaling (the “bounding” models category in Fig. 1).

The second strategy employs a range of bias correction methods to reduce errors in the GCM outputs. Univariate bias correction methods are widely used to improve agree-

ment of the statistical attributes (mean, variance, quantiles) of the simulated climate variables with those of historical climate data. While these methods can produce reasonable results (e.g., Yang et al., 2015; Casanueva et al., 2018) they typically correct each climate variable independently, one grid cell at a time. This can result in inconsistent relationships across physically interlinked climate variables and/or across a spatial domain. Given univariate methods do not account for multidimensional dependencies, they cannot correct temporal, inter-variable or spatial aspects of the simulations (François et al., 2020). To address these gaps, multivariate methods account for dependencies between variables and spatial patterns. Multivariate methods are especially valuable in impact modeling frameworks where the combination of atmospheric processes across a range of timescales and spatial scales, such as coinciding low rainfall and high temperatures inducing vegetation drought stress, are important (Zscheischler et al., 2019).

Finally, several weighting methods have been developed to derive ensemble averages. The arithmetic multi-model mean is commonly used (Knutti et al., 2010a), and by canceling non-systematic errors it usually outperforms individual GCMs. However, assigning each ensemble member a uniform weight has been criticized (Knutti et al., 2010b; Herger et al., 2019). Nonuniform weights, based on skill, independence, or skill and independence combined (e.g., Bishop and Abramowitz, 2013; Brunner et al., 2019, 2020), can also be used. In addition, machine learning techniques have become increasingly popular to calculate multi-model averages (e.g., Huntingford et al., 2019; Thao et al., 2022) that use GCM outputs as predictors to match an observation-based target (e.g., reanalysis products). For example, Wang et al. (2018) explored a random forest approach, support vector machine, and Bayesian model averaging to calculate a best-fit multi-model ensemble average for monthly temperature and precipitation over Australia. Similarly, other studies have focused on climate extremes (e.g., Deo and Şahin, 2015; Liu et al., 2016) and climate impacts on the environment (e.g., Jung et al., 2010; Yang et al., 2016; C. Wu et al., 2019) using machine learning approaches.

In this study, we focus on Australia, and analyze the impact of climate forcing bias correction and ensemble-averaging methods on the simulated historical carbon cycle. Australia is a suitable study system for this work because climate projections of precipitation will remain uncertain at regional scales for the foreseeable future (IPCC, 2013; Ukkola et al., 2020; Grose et al., 2020). These uncertainties are likely to have a disproportionate influence on water-limited regions such as Australia, with potential impacts on vegetation distributions and water and carbon cycles, given many biologically relevant processes are threshold-based and disproportionately responsive to extremes as opposed to midrange changes in climate forcing. While Australia is not the largest contributor to the global carbon sink on centennial timescales, the continents' total carbon storage is still significant. On

shorter timescales, the interannual variability (IAV) in net biome productivity (NBP) is important for the both historical and future estimates of atmospheric growth rate since several studies (e.g., Poulter et al., 2014; Ahlström et al., 2015) have found that Australia can be a major contributor to the global net carbon sink in wet years. It is therefore important to reduce the uncertainty in carbon cycle projections over Australia, first to improve estimates of future carbon sinks, second to help constrain future atmospheric growth rates, and third because the improved understanding will ultimately enable better predictions of vegetation responses and of fire to climate change over Australia. Here, we assess the impact of different Coupled Model Intercomparison Project 6 (CMIP6) GCM selection, bias correction, and ensemble-averaging methods on the simulated carbon cycle in a synthetic experiment. We use a single dynamic global vegetation model, LPJ-GUESS (Smith et al., 2014), forced with different versions of CMIP6 climate forcing, as well as LPJ-GUESS forced with the CRUJRA reanalysis (Harris, 2019), as a target dataset for the carbon variables and focus on responses at seasonal to centennial timescales. Using a single model forced with multiple realizations of climate allows us to separate climate-driven uncertainties from those arising from model parametrizations. LPJ-GUESS belongs to an emerging second generation of DGVMs, i.e., it is a cohort-based DGVM that incorporates the dynamics of forest gap models. It can therefore be expected to simulate more realistic temporal carbon dynamics than first-generation DGVMs, which typically rely on a single area-averaged representation of each plant functional type (PFT) for each climatic grid cell (e.g., Fisher et al., 2018). Our goal is to examine how the choice of method to deal with climate biases and uncertainty in the CMIP6 climate forcing influences the projection of the terrestrial carbon cycle and whether any selected method represents a robust or preferable choice.

## 2 Climate forcing

### 2.1 CMIP6

We chose the historical simulations of 21 CMIP6 GCMs (see Table 1) that provide the three meteorological forcing variables needed to run LPJ-GUESS, i.e., the near-surface air temperature (*tas*), the total precipitation flux (*pr*), and the incoming shortwave radiation (*rsds*), and examine the *r1i1p1f1* realization that covers the time period 1850–2100. Four GCMs (ACCESS-CM2, ACCESS-ESM1-5, BCC-CSM2-MR, and NESM3) provide incoming shortwave radiation starting in 1950 only. For these GCMs, we recycled the climate forcing of the first 25 years of the available forcing (i.e., 1950–1974) for the first 100 years (i.e., 1850–1949). All GCMs provide daily data but differ in their spatial resolution. We therefore regridded all GCMs to a common 0.5° grid using first-order conservative remapping to match

the resolution of the reanalysis and the native grid of LPJ-GUESS and focus on the historical time period (1901–2019).

## 2.2 Reanalysis

We chose the CRUJRA reanalysis product (Harris, 2019) as the reference dataset to compare with the unconstrained CMIP6 results, as well as to derive bias corrections and ensemble weights. In addition, we use LPJ-GUESS runs forced with the CRUJRA reanalysis as reference datasets for carbon variables. CRUJRA is derived from the Climatic Research Unit gridded Time Series (CRU TS) v4.03 monthly data (Harris et al., 2014) and from the Japanese 55-year Reanalysis data (JRA-55) (Kobayashi et al., 2015). Temperature, downward solar radiation flux, specific humidity, and precipitation in JRA-55 are aligned to temperature, cloud fraction, vapor pressure, and precipitation in CRU TS (v4.03), respectively. The CRUJRA dataset spans the years 1901–2018 on a 6 h time step, which we aggregated to a daily temporal resolution at a 0.5° spatial resolution.

## 2.3 Dataset sensitivity

The CRUJRA reanalysis is not “observations” and, as with all reanalyses, is subject to uncertainty itself. To test the sensitivity to the choice of reference dataset, we compared the CRUJRA to the ERA5 reanalysis dataset.

ERA5 is the fifth-generation reanalysis from the European Centre for Medium-Range Weather Forecasts (ECMWF; Hersbach et al., 2020). It uses a linearized quadratic 4D-Var assimilation scheme that takes the timing of the observations and model evolution within the assimilation window into account. Compared to the predecessor ERA-Interim reanalysis, it has a higher spatiotemporal resolution and assimilates more observations. The reanalysis is produced at an hourly time step and covers the time period 1979–2020. Its horizontal resolution is 0.1°. As for the CRUJRA reanalysis, we aggregated the data to a daily time step and regridded the dataset to a 0.5° spatial resolution using first-order conservative regridding.

## 2.4 Atmospheric CO<sub>2</sub> forcing and nitrogen deposition

In addition to the climate forcing, both atmospheric CO<sub>2</sub> concentration and nitrogen deposition are transient. We force LPJ-GUESS with the atmospheric CO<sub>2</sub> forcing following historical data until the year 2014. For the remaining years, values for the shared socio-economic pathway SSP245 are used (both from Meinshausen et al., 2020). We further prescribe historical nitrogen deposition until 2009. After 2009, LPJ-GUESS is forced with the nitrogen deposition following the representative concentration pathway RCP4.5 (based on Lamarque et al., 2013).

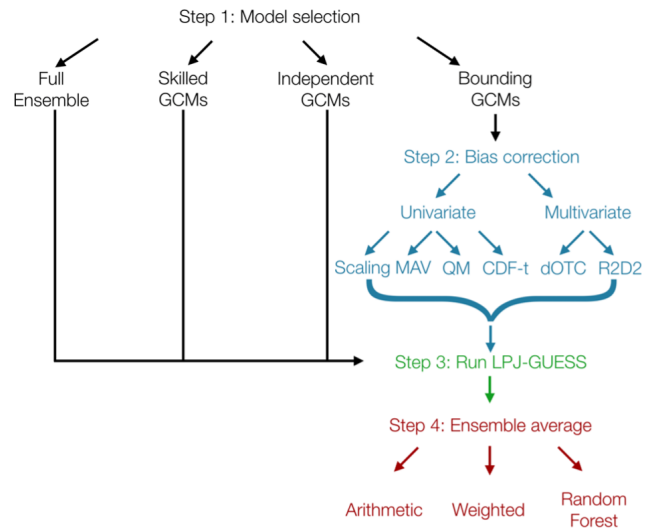


**Figure 1.** Schematic for study setup. All terms are defined in the text, and the key steps are also described in the text. GCM refers to Global circulation models. MAV, QM, CDF-t, dOTC, and R2D2 represent five different bias correction methods (mean and variance, quantile mapping, cumulative distribution function, dynamical optimal transport correction, and rank resampling for distributions and dependences, respectively).

## 3 Methods

To assess the sensitivity of carbon cycle projections to different GCM selection, bias correction, and ensemble-averaging methods, we followed the steps outlined in Fig. 1 and detailed below.

### 3.1 Step 1: model selection

Our first step was to decide whether to use the full CMIP6 ensemble (“full ensemble”) or to select a subset of GCMs based on a selection criterion (“skilled”, “independent”, “bounding”; see Fig. 1 step 1 and Fig. A1 in the Appendix). Since precipitation is the single largest driver of variability in the Australian carbon cycle (Haverd et al., 2013), we selected the GCMs solely based on the performance of projected precipitation. We next describe each of the selection criteria in more detail (see Fig. 1 step 1).

#### 3.1.1 Skilled GCMs

An intuitive way to select CMIP GCMs is to define a set of performance metrics and select those GCMs with a predefined level of skill (e.g., Rowell et al., 2016; Gershunov et al., 2019). We calculated the metrics suggested by Houghton et al. (2018) (see Table 2) using the CRUJRA reanalysis as the reference dataset for daily, monthly, and annual precipitation; ranked all GCMs for each metric; and finally chose the GCMs with the highest average rank for monthly and annual timescales. For the last method (overlap of histogram),

**Table 1.** CMIP6 models used to force LPJ-GUESS. Further details for each model are available at the references listed in this table.

GCM	Institute ID	Native resolution (lat × long)	Key reference
ACCESS-CM2	CSIRO-ARCCSS	1.25° × 1.875°	Bi et al. (2013)
ACCESS-ESM1-5	CSIRO	1.25° × 1.875°	Law et al. (2017)
BCC-CSM2-MR	BCC	1.121° × 1.125°	T. Wu et al. (2019)
CanESM	CCCma	2.7905° × 2.8125°	Swart et al. (2019)
CESM2-WACCM	NCAR	1.3° × 0.9°	Liu et al. (2019)
CMCC-CM2-SR5	CMCC	0.94° × 1.25°	Cherchi et al. (2019)
EC-Earth3	EC-Earth-Consortium	~0.7° × 0.7°	Döscher et al. (2022)
EC-Earth3-Veg	EC-Earth-Consortium	~0.7° × 0.7°	Döscher et al. (2022)
GFDL-CM4	NOAA-GFDL	1° × 1.25°	Held et al. (2019)
GFDL-ESM4	NOAA-GFDL	1° × 1.25°	Dunne et al. (2020)
INM-CM4-8	INM	1.5° × 2°	Volodin et al. (2018)
INM-CM5-0	INM	1.5° × 2°	Volodin et al. (2018)
IPSL-CM6A-LR	IPSL	1.3° × 2.5°	Boucher et al. (2020)
KIOST-ESM	KIOST	1.875° × 1.875°	Pak et al. (2021)
MIROC6	MIROC	1.4° × 1.4°	Tatebe et al. (2019)
MPI-ESM1-2-HR	MPI-M	0.94° × 0.94°	Mauritsen et al. (2019), Müller et al. (2018)
MPI-ESM1-2-LR	MPI-M	1.865° × 1.875°	Mauritsen et al. (2019)
MRI-ESM2-0	MRI	1.121° × 1.125°	Yukimoto et al. (2019)
NESM3	NUIST	1.865° × 1.875°	Cao et al. (2018)
NorESM2-LM	NCC	1.9° × 2.5°	Seland et al. (2020)
NorESM2-MM	NCC	0.94° × 1.25°	Seland et al. (2020)

**Table 2.** Metrics used to evaluate GCM performance (compare Haughton et al., 2018).  $O$  is the observation, here the reanalysis, and  $S$  is the simulation.

Metric	Formulation
Mean bias error	$\frac{1}{n} \sum_{i=1}^n \frac{S_i - O_i}{n}$
Difference in standard deviation	$ 1 - \frac{\sigma_S}{\sigma_O} $
Correlation	$\text{corr}(O, S)$
Difference in 5th percentile	$P_5(S) - P_5(O)$
Difference in 95th percentile	$P_{95}(S) - P_{95}(O)$
Difference in skewness	$\left 1 - \frac{\text{skew}(S)}{\text{skew}(O)}\right $
Difference in kurtosis	$\left 1 - \frac{\text{kurt}(S)}{\text{kurt}(O)}\right $
Overlap of histogram	$\sum(\min(\text{bin}_{S,k}, \text{bin}_{O,k}))$

we estimated the intervals (“bin size”) using the Freedman–Diaconis estimator (Freedman and Diaconis, 1981) for the reference dataset (CRUJRA) and then used the same bin size for the simulated variable (i.e., CMIP forcing).

### 3.1.2 Independent GCMs

The CMIP6 ensemble is not designed to be an ensemble of independent models, and therefore there is a risk that the members of the ensemble share systematic biases. We there-

fore seek to select GCMs that are independent of each other, in order to obtain a better sample of model projections. Here we defined that GCMs are independent if their (in this case, precipitation) biases are uncorrelated with any of the other ensemble members. We derived the bias by subtracting the reanalysis from the simulated precipitation and then calculated the Pearson correlation coefficient between the different CMIP6 GCMs on monthly and annual timescales and chose the GCMs with a weak correlation coefficient (i.e., lower than 0.3; cf. Bishop and Abramowitz, 2013). While 0.3 is an arbitrary threshold, it is commonly interpreted to represent weak to moderate correlation. We further note that multiple approaches exist to define GCM dependence (see, for example, Knutti et al., 2010a; Herger et al., 2019), and following a different method may yield a different result. Moreover, reanalysis products and GCMs can share modules as well, which further complicates achieving an estimate of truly independent GCMs.

### 3.1.3 Bounding GCMs

Similar to Evans et al. (2014), we also chose GCMs that span the largest range of simulated precipitation based on the average, the interannual variability (IAV) and the change of average precipitation in the last 30 years of the historical time period (1989–2018) compared to 1901–1930. Accordingly, the five bounding GCMs are the driest (INM-CM4-8) and the wettest (MPI-ESM1-2-HR) GCM, the GCMs with the lowest (KIOST-ESM) and highest (NorESM-MM) IAV in precipita-

tion and the GCMs with the lowest (EC-Earth3-Veg) and the highest (NorESM2-MM) change of average precipitation in 1989–2018 relative to the 1901–1930 average.

### 3.2 Step 2: bias correction methods

Once a selection of GCMs is made, the biases of a given GCM can be corrected (see Fig. 1 step 2). We explored six approaches using CRUJRA as our reference dataset. We corrected the three climate forcing variables, i.e., temperature, precipitation, and incoming shortwave radiation, and derived the correction based on the calibration time period 1989–2010 given this is common to both reanalysis products used here. We applied each method per pixel so that the different grid points were corrected independently of each other and tested the correction on both daily and monthly timescales, and we note that none of the correction methods used here are designed to correct temporal properties of the climate forcing. We show the corrections based on daily timescales in the main figures and use the corrections based on monthly timescales to assess the sensitivity to the correction timescale in the Supplement. To understand the sensitivity to the correction technique, we only corrected the five bounding models (see Sect. 3.1.3) because they defined the total CMIP6 ensemble spread. In the subsections below, we describe the methods in more detail. In the following,  $O$  and  $S$  represent the observed and simulated variables at the same grid point for the calibration time period.  $P$  is the simulated variable for the projection period to adjust with bias correction methods, and  $C$  is the resulting bias-corrected variable. The projection period was split into 10 separate 25-year slices. The bias correction was then derived and applied to each calendar month on a daily time step within each time slice separately. Let  $P_t$  and  $C_t$  be the values of the variables at time  $t$ .

#### 3.2.1 Scaling

We calculated additive (temperature) and multiplicative (precipitation and incoming shortwave radiation) scaling bias corrections based on the 1989–2010 climatology (compare, e.g., Chen et al., 2011). For temperature, the bias-corrected value at time  $t$  for the projection period is derived as follows:

$$C_t = P_t - \bar{S} + \bar{O}, \quad (1)$$

with  $\bar{S}$  and  $\bar{O}$  the means of the variables  $S$  and  $O$ , respectively. For precipitation and incoming shortwave radiation, bias-corrected values are derived according to

$$C_t = \frac{P_t}{\bar{S}} \cdot \bar{O} \quad (2)$$

to avoid negative values.

#### 3.2.2 Mean and variance correction (MAV)

Here, we aimed to additionally correct the variance in the temperature forcing. We followed Eq. (1) and accounted for

the variance by multiplying by the ratio between the standard deviation of the observed and simulated variables  $\sigma_O$  and  $\sigma_S$ . The forcing variables are corrected following

$$C_t = (P_t - \bar{S}) \cdot \frac{\sigma_O}{\sigma_S} + \bar{O}. \quad (3)$$

We used the precipitation and incoming shortwave radiation corrected following the multiplicative correction (see Eq. 2) since the (proportional) scaling correction affects both mean and variance.

#### 3.2.3 Quantile mapping (QM)

We employed the univariate quantile mapping (QM) method (Panofsky et al., 1958; Wood et al., 2004; Déqué, 2007), which adjusts the cumulative distribution function of a modeled climate variable to that of the observed one. Let  $F_O$  and  $F_S$  denote the cumulative distribution function (CDF) of the observed and simulated variables, respectively. By linking CDFs between the model and the reference, the QM method allows us to derive the bias-corrected value  $C_t$  as follows:

$$C_t = F_O^{-1}(F_S(P_t)), \quad (4)$$

where  $F_O^{-1}$  is the inverse cumulative distribution function of  $O$ .

#### 3.2.4 Cumulative distribution function (CDF-t)

The “cumulative distribution function – transform” (CDF-t; Michelangeli et al., 2009) method is a version of quantile mapping that adjusts the cumulative distribution function of the simulated climate variables using a quantile-mapping transfer function. The difference with QM is that, by linking cumulative distribution functions using a two-step procedure, CDF-t is specifically designed to take into account the simulated changes of CDFs from the calibration to the projection period. Thus, the future climate scenarios incorporate the model's projected changes in both mean climate and variability at all timescales up to the decadal. More details can be found in Vrac et al. (2012). Implementing the CDF-t method in the present study in addition to the QM method allows us to assess the influence of taking into account simulated distribution changes in the bias correction procedure on results of regional projections of carbon cycle for Australia.

#### 3.2.5 Dynamical optimal transport correction (dOTC)

The “dynamical optimal transport correction” method (dOTC, Robin et al., 2019) is a generalization of the CDF-t method to the multivariate case. By using optimal transport theory, dOTC is designed to adjust both univariate distributions and dependence structures of the simulated variables. Moreover, following the philosophy of CDF-t, dOTC is able to preserve not only the simulated changes in the univariate

distributions between the calibration and the projection periods but also the simulated change in multivariate properties (e.g., induced by climate change). For more details and equations, see Robin et al. (2019) and François et al. (2020).

### 3.2.6 Rank resampling for distributions and dependences (R2D2)

The “rank resampling for distributions and dependences” method (“R2D2”, Vrac, 2018) is based on the Schaake Shuffle (Martyn Clark et al., 2004). The Schaake Shuffle is a re-ordering technique that reorders a sample so that its rank structure corresponds to the rank structure of a reference sample. This allows the reconstruction of multivariate dependence structures. As a first step, the R2D2 performs the univariate CDF-t bias correction (see Sect. 3.2.4). The method allows for the possibility to select a “reference dimension” for the Schaake Shuffle, i.e., one physical variable at one given site, for which rank chronology remains unchanged. The reconstruction of inter-variable correlations of the reference is then performed using the Schaake Shuffle with the constraint of preserving the rank structure for the reference dimension. For more details and equations, see Robin et al. (2019) and François et al. (2020).

### 3.3 Step 3: run LPJ-GUESS

We ran LPJ-GUESS with a reference dataset (CRUJRA reanalysis), the full raw CMIP6 ensemble (which includes the skilled, independent, and bounding models) and additionally with the bounding models (see Sect. 3.1.3) after they were bias-corrected according to the methods described in Sects. 3.2.1–3.2.6.

LPJ-GUESS (Smith et al., 2014; Lund–Potsdam–Jena General Ecosystem Simulator) is a widely used dynamic global vegetation model for climate–carbon studies (Sitch et al., 2003; Smith et al., 2014). LPJ-GUESS simulates the exchange of water, carbon, and nitrogen through the soil–plant–atmosphere continuum (Smith et al., 2014) by accounting for resource competition for light and space between plants. We adopted the global configuration of the model that uses 12 plant functional types (PFTs), simulating differences in growth form (grasses, broadleaved trees, or deciduous trees), photosynthetic pathway ( $C_3$  or  $C_4$ ), phenology (evergreen, summer green, or rain green), tree allometry, life history strategy, fire sensitivity, and bioclimatic limits for establishment and survival (see Smith et al., 2014, for details). LPJ-GUESS is a second-generation DGVM part of the TRENDY ensemble (compare Fisher et al., 2010, 2018) and explicitly represents demographic processes, such as stand age and size structure development, mortality, and competition, among locally co-occurring PFT populations, as well as disturbance-induced heterogeneity across the landscape of a grid cell.

We use LPJ-GUESS version 4.0.1 in “cohort mode”, where woody plants of the same size and age co-occur in a “patch” and, as such, are represented by a single average individual. Each PFT is represented by multiple average individuals, and one PFT cohort is defined as the average of several individuals. We run LPJ-GUESS with the plant and soil nitrogen dynamics switched on. Fire is simulated annually (stochastically) based on temperature, fuel availability, and the moisture content of upper soil layer as a proxy for litter moisture content (Thonicke et al., 2001).

### 3.4 Step 4: ensemble averages

After running LPJ-GUESS with either the raw or corrected climate data (step 3), the final step was to calculate an ensemble average of the resulting carbon fluxes. We focused on the total carbon storage ( $C_{\text{Total}}$ ) and foliar projective cover (FPC) over Australia at annual time steps and the gross primary productivity (GPP) at seasonal time steps. We explored three different approaches based on the full ensemble or the selected models (see Sect. 3.1)

#### 3.4.1 Arithmetic ensemble average

We first calculated the arithmetic ensemble average where each of the GCM+LPJ-GUESS ensemble members was assigned the same weight.

#### 3.4.2 Skill and independence

Following Bishop and Abramowitz (2013), we calculated weights based on both independence and skill. We here chose the carbon variables resulting from the reference LPJ-GUESS run (driven with the CRUJRA reanalysis) as the target variable, and the carbon variables resulting from the LPJ-GUESS runs forced with the CMIP6 as the predictor variables. This method accounts for both the performance differences and their error dependencies. In a first step, the bias with respect to observational data is calculated. Then, the error correlation coefficient is used as a metric for error dependencies. The linear combination of the CMIP6 members is derived to minimize the mean square difference to the results from the reanalysis runs following:

$$C_w^j = w^T x^j = \sum_{k=1}^K w_k x_k^j, \quad (5)$$

where  $j$  represents the grid cells and  $k$  is the number of the ensemble members. Consequently,  $x_k^j$  is the value of the  $k$ th bias-corrected model (i.e., after subtracting the mean error from the dataset) at the  $j$ th grid cell. The weights ( $w^T$ ) provide an analytical solution to the minimization of

$$\sum_{j=1}^J (C_w^j - x_{\text{obs}}^j)^2, \quad (6)$$

when subject to the constraint that the sum of the weights ( $w_k$ ) always adds up to 1. The solution can be expressed as follows:

$$w = \frac{\mathbf{A}^{-1}\mathbf{1}}{\mathbf{1}^T\mathbf{A}^{-1}\mathbf{1}}, \quad (7)$$

where  $\mathbf{1}^T = \overbrace{[1, 1, \dots, 1]}^{k \text{ elements}}$  and  $\mathbf{A}$  is the  $K \times K$  difference covariance matrix.

### 3.4.3 Random forest

Random forest is an ensemble learning method that constructs a collection of decision trees and then outputs a weighted average of predictions of the individual trees. For each decision tree, a subset of training samples are randomly selected following a bootstrap sampling approach. At each node, a random sample of predictor variables is selected for splitting. We varied the number of predictor variables and number of trees, and here we show the results that produced the lowest error. The metric of splitting is the sum of squares of errors. As in Sect. 3.4.2, we chose the carbon variables resulting from the reference LPJ-GUESS run (driven with the CRUJRA reanalysis) as the target variable and the carbon variables resulting from the LPJ-GUESS runs forced with the CMIP6 as the predictor variables. We further included the latitude and longitude as predictors and, when analyzing monthly data, the month. The random selections change as the “tree” grows following a random sampling with the replacement approach. The algorithms involved in different decision trees are run in parallel. Both the random sampling procedure and the parallelism in algorithm operations mean that the predictor blocks in random forest are built independently.

### 3.5 Summary of methods

Our methods examine many of the approaches previously used to select from and/or constrain the CMIP6 ensemble in carbon cycle modeling. In this study, we seek to examine how applying these corrections methods affects the simulation of the Australian carbon cycle by LPJ-GUESS as a case study. In the following, we use the abbreviations defined in Table 3.

## 4 Results

We first explored the uncertainty in the CMIP6 climate fields by examining the average and IAV (depicted by the standard deviation of the detrended annual precipitation and temperature) of the simulated and reanalysis annual precipitation and temperature over Australia between 1989 and 2018 (see Fig. 2). Annual precipitation (1989–2018) simulated by the CMIP6 ensemble members varies widely from

254 mm yr<sup>-1</sup> (MPI-ESM1-2-HR) to 858 mm yr<sup>-1</sup> (INM-CM4-8). The CRUJRA reanalysis lies in the lower quartile of the CMIP6 spread (499 mm yr<sup>-1</sup>; see Fig. 2c), implying a systematic overestimate across the CMIP6 GCMs. The precipitation IAV varies between 55 mm yr<sup>-1</sup> (KIOST-ESM) and 183 mm yr<sup>-1</sup> (NorESM2-MM), and most CMIP6 ensemble members simulated higher IAV than the CRUJRA reanalysis (66 mm yr<sup>-1</sup>; see Fig. 2c). Relative to 1901–1930, most CMIP6 GCMs do not show a significant trend (17 out of 21), two GCMs significantly increase in precipitation (up to 76 mm yr<sup>-1</sup> at the end of the historical time period; NorESM2-MM) and two GCMs significantly decrease (down to -59 mm yr<sup>-1</sup>, EC-Earth3-Veg). CRUJRA slightly increases in precipitation relative to 1901–1930 for the latter half of the historical time period (27.2 mm with a significant trend of 0.40 mm yr<sup>-1</sup>; see Fig. 2d).

The average simulated temperature over Australia for the last 30 years of the historical time period varies amongst the CMIP6 ensemble members from 21.2 °C (INM-CM5-0) up to 24.6 °C (MIROC6). The median of the full ensemble is 22.7 °C and slightly higher than the average temperature for the CRUJRA reanalysis (22.1 °C). The IAV in temperature ranges from 0.27 °C (NorESM-LM) to 0.68 °C (GFDL-ESM4). The CMIP6 GCMs tend to simulate higher IAV in temperature compared to the year-to-year variability found in the CRUJRA reanalysis (0.31 °C; see Fig. 2a). Relative to 1901–1930, all CMIP6 ensemble members show a continental average increases in temperature but to varying degrees (~0.4–1.2 °C averaged over 1989–2018; see Fig. 2b). We note that Fig. 2b, d, and f show the smoothed change in the according variable and do not allow conclusions on IAV.

Finally, Fig. 2e and f show the impact of differences in the meteorological forcing on the average simulated total carbon pool ( $C_{\text{Total}}$ ), the IAV in net biome productivity (NBP), and the change in  $C_{\text{Total}}$  for Australia when LPJ-GUESS is forced with the raw climate forcing of each of the CMIP6 ensemble members. Depending on the choice of GCM,  $C_{\text{Total}}$  varies between 28.6 PgC (LG<sub>MPI-ESM1-2-HR</sub>) and 75.1 PgC (LG<sub>INM-CM4-8</sub>). Compared to  $C_{\text{Total}}$  simulated by LG<sub>CRUJRA</sub> (56.4 PgC), the LPJ-GUESS driven with CMIP6 forcing tends to simulate lower  $C_{\text{Total}}$ . The IAV in NBP ranges between 0.3 PgC (LG<sub>KIOST-ESM</sub>) and 1.1 PgC (LG<sub>CMCC-CM2-SR5</sub>). The IAV in NBP simulated by LG<sub>CRUJRA</sub> (0.6 PgC) falls into the lower interquartile range (IQR) of the CMIP6 ensemble runs.  $C_{\text{Total}}$  for Australia increases by the end of the historical period for all CMIP6 forcings with values between 0.1 PgC (LG<sub>EC-Earth3</sub>) and 4.1 PgC (LG<sub>NorESM2-MM</sub>). Compared to the reanalysis results, most of the CMIP6 models lead to a weaker increase in  $C_{\text{Total}}$  over the historical period (except for LG<sub>INM-CM4-8</sub>, LG<sub>INM-CM5-0</sub>, LG<sub>NorESM2-LM</sub>, and LG<sub>NorESM2-MM</sub>).

Taken together, Fig. 2 demonstrates both the uncertainties in meteorological variables obtained from GCMs and how these propagate to large simulation biases in Australia's car-



**Table 3.** List of LPJ-GUESS runs and ensemble-averaging methods tested in this study.

Run	Climate input used to force LPJ-GUESS	Ensemble abbreviation	Averaging method	Based on
LGCRUJRA	CRUJRA reanalysis	ENS <sub>Arithmetic,Full</sub>	Arithmetic	Full CMIP6 ensemble (raw)
LGEC-Earth3-Veg	Raw EC-Earth3-Veg climate	ENS <sub>Arithmetic,Skill</sub>	Arithmetic	Skilled GCMs (raw)
LGINM-CM4-8	Raw INM-CM4-8 climate	ENS <sub>Arithmetic,Independence</sub>	Arithmetic	Independent GCMs (raw)
LGKIOST-ESM	Raw KIOST-ESM climate	ENS <sub>Arithmetic,Bounding</sub>	Arithmetic	Bounding GCMs (raw)
LGMPLESM1-2-HR	Raw MPI-ESM1-2-HR climate	ENS <sub>Arithmetic,Bounding,Scaling</sub>	Arithmetic	Corrected bounding GCMs (scaling)
LGNorESM2-MM	Raw NorESM2-MM climate	ENS <sub>Arithmetic,Bounding,MAV</sub>	Arithmetic	Corrected bounding GCMs (MAV)
		ENS <sub>Arithmetic,Bounding,QM</sub>	Arithmetic	Corrected bounding GCMs (QM)
		ENS <sub>Arithmetic,Bounding,CDF-t</sub>	Arithmetic	Corrected bounding GCMs (CDF-t)
		ENS <sub>Arithmetic,Bounding,R2D2</sub>	Arithmetic	Corrected bounding GCMs (R2D2)
		ENS <sub>Arithmetic,Bounding,dOTC</sub>	Arithmetic	Corrected bounding GCMs (dOTC)
		ENS <sub>Weighted</sub>	Weighted	Full CMIP6 ensemble (raw)
		ENS <sub>RF</sub>	Random forest	Full CMIP6 ensemble (raw)

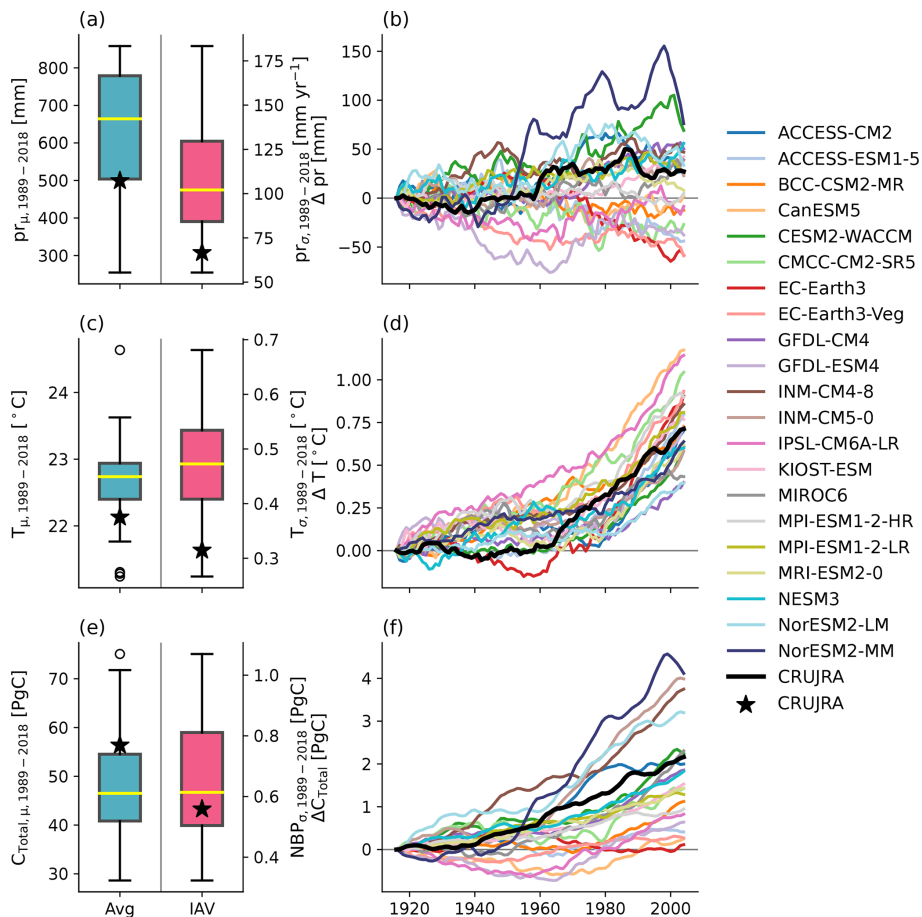


**Figure 2.** Average and interannual variability (IAV) of annual precipitation averaged over Australia for the time period 1989–2018 (a), average and IAV of annual temperature averaged over Australia for the time period 1989–2018 (c) for the 21 CMIP6 ensemble members (see Table 1). Panel (e) shows the average of the total carbon stored in Australia for the time period 1989–2018 based on LPJ-GUESS simulations with the CMIP6 ensemble on the left and the IAV of the net biome productivity over Australia for the same time period on the right. The black stars represent the respective values obtained using the CRUJRA reanalysis. Panels (b), (d), and (f) show the 30-year moving average of the change in annual temperature, precipitation, and total carbon storage, respectively, relative to the 1901–1930 average. The thick black line represents simulations obtained using the CRUJRA reanalysis.

bon cycle. In the following, we examine the impact of correcting climate forcing on these biases.

The large ensemble spread in the CMIP6 forcing variables (see Fig. 2a–d) results in a large spread in the simulated carbon cycle (see Fig. 2e and f). Figure 3a shows the biases in the forcing variables precipitation (pr) and temperature ( $T$ ) and  $C_{\text{Total}}$  based on the CMIP6 compared to the results of the reanalysis. Positive values indicate that the results based on the CMIP6 forcing are higher compared to the reanalysis, and negative values demonstrate the opposite. Each of the bias correction methods reduces the bias in the forcing variables so that the bias in the corrected precipitation is significantly lower, and thus the bias in corrected temperature in comparison to the raw CMIP6 meteorology is close to zero (see Fig. 3a, c). Consequently,  $C_{\text{Total}}$  based on LPJ-GUESS driven with the corrected CMIP6 GCMs results in a smaller distance to  $C_{\text{Total}}$  based on the LG<sub>CRUJRA</sub> run compared to the raw forcing for most LPJ-GUESS runs (see Fig. 3a). However, while the results based on the LG<sub>NorESM2-MM</sub> model initially simulated  $\sim 3$  PgC more than the runs based on the CRUJRA reanalysis, all univariate bias correction methods lead to larger biases from  $-5.0$  PgC (CDF-t) to  $-8.3$  PgC (scaling), while the multivariate methods result in biases similar in magnitude (dOTC) or reduce it significantly (R2D2). When averages are calculated based on the full CMIP6 ensemble (hollow circles in Fig. 3e), the random forest and weighted ensemble average approaches produce almost identical results compared to the LG<sub>CRUJRA</sub> run ( $-0.29$  and  $-0.16$  PgC, respectively; see Fig. 3). The arithmetic ensemble average of  $C_{\text{Total}}$  is with  $-7.7$  PgC lower than the weighted average and the random forest approach. Figure 3e also shows the impact of model selection on calculated ensemble averages. Given both the weighted ensemble-averaging and random forest approaches are insensitive to redundant (i.e., models with similar biases) information, we expect that testing those methods based on different GCM subsamples will yield similar results. We therefore only show the impact on the arithmetic average of  $C_{\text{Total}}$ . The values for the arithmetic average can depend on the selection of models it is derived from. Calculating the arithmetic average based on the full ensemble or on the five independent or bounding models gives similar results (but lower than the weighted and random forest approach, which give  $-9.0$ , and  $-7.6$  PgC, respectively). Notably, the arithmetic ensemble average based on the five most skilled models produces the lowest value of all selection methods ( $-18.9$  PgC). The arithmetic average of the bounding models is almost identical to that of the full ensemble for  $C_{\text{Total}}$  and does not change with the correction method (black hexagons in Fig. 3).

While the type of bias correction method only shows small alterations of the values of the arithmetic average of any of the variables examined in Fig. 3, the coefficient of variation (CV), which we here use as a measure for ensemble uncertainty, can vary depending on the method chosen. All bias correction methods reduce the CV compared to the

raw CMIP6 data. For temperature, all bias correction methods result in similar values for CV (see Fig. 3d). Precipitation shows some variation depending on the type of bias correction method applied (univariate vs. multivariate; see Fig. 3b). For temperature, the CV is robust and does not change strongly depending on the sub-selection of GCMs, while for precipitation, selecting GCMs with high skill decreases the CV most. The CV of  $C_{\text{Total}}$  is most reduced when the multivariate dOTC approach is applied on the forcing variables, and selecting the most skilled GCMs for an arithmetic average here yields the strongest reduction in CV compared to the full ensemble or selecting independent or bounding models.

Figure 4 shows the change in  $C_{\text{Total}}$  relative to the 1901–1930 average for the five bounding models (i.e., weakest and highest amount, change, and IAV in precipitation over time; see Figs. A3 and A2 for the corrected precipitation and temperature forcing). For the LPJ-GUESS runs based on the lowest amount in precipitation and increase in precipitation (LG<sub>EC-Earth3-Veg</sub> and LG<sub>MPI-ESM1-2-HR</sub>, respectively), none of the bias correction approaches significantly alter the change in  $C_{\text{Total}}$  so that the change in  $C_{\text{Total}}$  remains significantly lower compared to LG<sub>CRUJRA</sub> (see Fig. 4c and e). In the LPJ-GUESS runs forced with the highest annual precipitation (LG<sub>INM-CM4-8</sub>) and the strongest increase and highest IAV in precipitation (both LG<sub>NorESM2-MM</sub>), the bias correction methods generally reduce the simulated change of  $C_{\text{Total}}$  so that it is closer to the LG<sub>CRUJRA</sub> result (see Fig. 4a, b). For LG<sub>INM-CM4-8</sub>, all methods are successful in bias-correcting to the reanalysis. For LG<sub>NorESM2-MM</sub>, four methods approximately halve the difference between the reanalysis and raw runs, with the exception of CDF-t and dOTC. Figure 4f shows the impact of different ensemble-averaging methods applied to  $C_{\text{Total}}$ . All averaging methods simulate very similar  $\Delta C_{\text{Total}}$  values in the last 10 years of the model runs, whereas the weighted approach is lower by  $\sim 0.5$  PgC in the first 50 years.

Figure 5 shows the regional details of the relative differences between  $C_{\text{Total}}$  based on the three ensemble-averaging methods (full ensemble; a–c) and different model selection methods (d–e) compared to the reference run LG<sub>CRUJRA</sub>. The arithmetic (see Fig. 5a) and weighted average (see Fig. 5b) show regional biases that can be both positive (eastern central Australia) and negative (southwestern Australia) and along the Tropic of Capricorn. The random forest approach shows small differences in  $C_{\text{Total}}$  compared to the CRUJRA reanalysis. Figure 5 further supports that using a weighted average or random forest approach yields a more robust ensemble estimate than using the mean of any of the sub-ensembles. Deriving the arithmetic average based on the full ensemble or on a sub-selection based on independent or bounding models (see Fig. 5a, e, f) yields very similar results; notably, choosing the five most skilled models produces an overall negative bias in the  $C_{\text{Total}}$  estimate (see Fig. 5d).

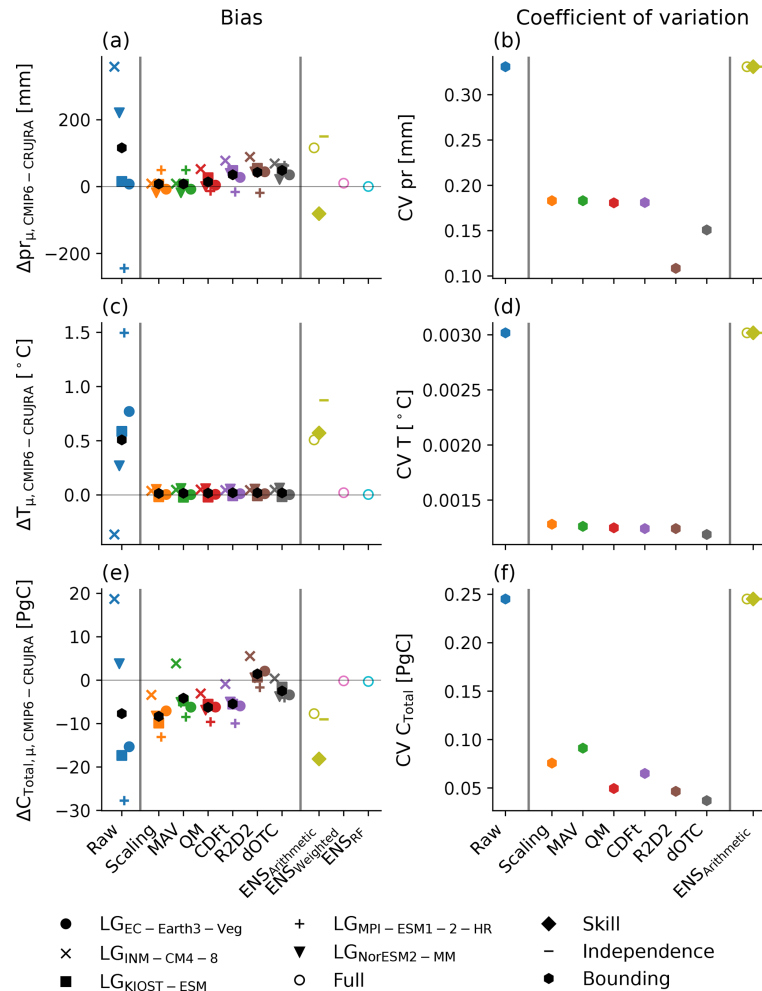


**Figure 3.** Difference between precipitation (pr), temperature ( $T$ ), and carbon storage ( $C_{Total}$ ) based on the CMIIP6 and CRUJRA forcing (a, c, e) and the coefficient of variance across the ensemble of the same variables averaged over Australia. The different colors represent the results based on the raw (blue) or corrected climate forcing using scaling (orange), mean and variance (MAV, green), quantile mapping (QM, red), cumulative distribution function – transform (CDF-t, purple), dynamical optimal transport correction (dOTC, brown), and matrix re-correlation (R2D2, dark grey) approaches and the three ensemble-averaging methods (arithmetic mean (olive), weighted average (pink), and random forest (cyan)). The different symbols show LPJ-GUESS runs forced with the five bounding models, i.e., EC-Earth3-Veg (filled circle), INM-CM4-8 (x), KIOST-ESM (square), MPI-ESM1-2-HR (+), and NorESM2-MM (triangle), the full ensemble (empty circle), and the three model selection methods, i.e., skill (diamond), independence (horizontal bar), and bounding models (hexagon). The black hexagons depict the ensemble average of the LPJ-GUESS runs based on the raw and corrected bounding climate forcing.

Correcting the bounding models tends to reduce the bias in the ensemble average of  $C_{Total}$  (see Fig. 5g–m). The resulting bias map for individual GCMs can depend on the raw simulation by the GCM to which the bias correction is applied. Each of the bias correction methods leads to similar spatial patterns within the same GCM (see Fig. A4).

Figure 6 shows the coefficient of variation (CV) of  $C_{Total}$  across the ensemble. Selecting either the full ensemble or making a sub-selection based on skill and independence (see Fig. 6a–c) results in a high CV across the Tropic of Capricorn that results from the assumed bioclimatic limit for  $C_4$  grasses (similar to Fig. 5). Selecting models based on skill (see Fig. 6a) reduces the CV compared to the full ensemble,

while choosing the five bounding models reduces the CV across the Tropic of Capricorn but increases it in most of the other regions. The CV is significantly lower when the climate forcing input is bias-corrected for all methods, and the quantile mapping approach overall leads to the lowest values.

The different patterns in  $\Delta C_{Total}$  for the bounding model runs imply that the underlying vegetation composition might vary with the climate forcing and the bias correction method applied. Indeed, studies have suggested that the sensitivity to climate forcing is generally larger on regional and PFT scales (Wu et al., 2017). To examine the impact of bias correction on vegetation composition, we examine the FPC, which can be seen as an indicator for the vegetation growth (due to the

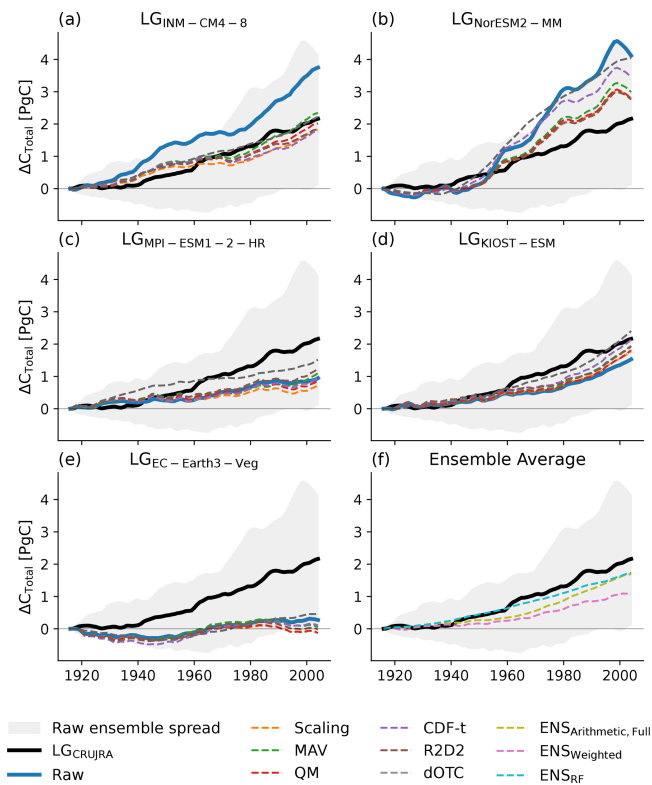


**Figure 4.** The 30-year moving average of the change in  $C_{\text{Total}}$  averaged over Australia. In each panel, the bold black line is the change in  $C_{\text{Total}}$  obtained using the CRUJRA reanalysis and the grey-shaded area represents the full unconstrained CMIP6 model ensemble. Panels (a)–(e) show the  $C_{\text{Total}}$  change simulated using input from the five individual bounding models separately. The colors show the change in  $C_{\text{Total}}$  based on the different bias correction methods. Panel (f) shows the change in  $C_{\text{Total}}$  estimated by the ensemble-averaging methods.

relationship between foliar area and light interception), and species competition through tree–grass shading. We focus on the FPC of four different vegetation groups (temperate and tropical trees and  $C_3$  and  $C_4$  grasses) for the five bounding models and different ensemble averages (see Fig. 7). For temperate trees, most raw models simulate a higher median compared to the FPC based on  $LG_{\text{CRUJRA}}$  (except for MPI-ESM1-2-HR; see Fig. 7a), and the variability in simulated FPC depends strongly on the GCM used to drive LPJ-GUESS. For the LPJ-GUESS runs based on the wettest GCM ( $LG_{\text{INM-CM4-8}}$  and the one based on the strongest increase in precipitation ( $LG_{\text{NorESM2-MM}}$ ), the median falls outside the  $LG_{\text{CRUJRA}}$  interquartile range, and the 75th percentile of both models is more than double ( $LG_{\text{MPI-ESM1-2-HR}}$ ) or triple ( $LG_{\text{INM-CM4-8}}$ ) of what the  $LG_{\text{CRUJRA}}$  run suggests. For all models, correcting the GCM forcing brings the simulated FPC much closer together. The arithmetic and weighted ensemble average result in a higher median and 25th and 75th percentile compared to the  $LG_{\text{CRUJRA}}$  run. The median of the

random forest run is close to the  $LG_{\text{CRUJRA}}$  median. However, the 75th percentile is significantly lower compared to that of  $LG_{\text{CRUJRA}}$ , and the variability for the random forest approach is overall lower compared to  $LG_{\text{CRUJRA}}$ . Only choosing skilled models reduces the median of the arithmetic ensemble average, leading to better agreement with the  $LG_{\text{CRUJRA}}$  reanalysis, but the variability is lower. The other selection methods produce similar values for the median compared to the full ensemble result with a larger spread.

For the tropical trees (see Fig. 7b), most models simulate medians and interquartile ranges similar to that based on the  $LG_{\text{CRUJRA}}$  reanalysis. In contrast, the FPC based on wettest GCM ( $LG_{\text{INM-CM4-8}}$ ) shows a significantly higher median and 75th percentile (the latter being about 4 times higher than  $LG_{\text{CRUJRA}}$ ). All bias correction methods decrease the median so that it is within the  $LG_{\text{CRUJRA}}$  interquartile range (IQR). The MAV approach, however, still leads to a 75th percentile that is too high. The weighted ensemble average shows the distribution that is the most similar compared to the  $LG_{\text{CRUJRA}}$  FPC. Calculating the arithmetic average based on the full ensemble yields a similar result; however, the random forest approach median almost drops out of the  $LG_{\text{CRUJRA}}$  IQR. The arithmetic approach based on the independent GCMs produce the best match compared to  $LG_{\text{CRUJRA}}$ .

In contrast to the two tree groups, the median  $C_3$  grass FPC based on the CMIP6 forcing tends to be lower than that based on  $LG_{\text{CRUJRA}}$  (see Fig. 7). The  $C_4$  grasses show a mixed response to the raw CMIP6 forcing. The LPJ-GUESS runs based on the wettest model and the one with the strongest increase in precipitation ( $LG_{\text{INM-CM4-8}}$  and  $LG_{\text{NorESM2-MM}}$ ) simulate a higher median FPC compared to the  $LG_{\text{CRUJRA}}$ , while the runs based on the driest model and the model with the lowest increase in precipitation ( $LG_{\text{MPI-ESM1-2-HR}}$  and  $LG_{\text{EC-Earth3-Veg}}$ ) are lower. The  $LG_{\text{MPI-ESM1-2-HR}}$  run shows especially large variation in simulated  $C_4$  grass FPC depending on the correction method. For  $LG_{\text{INM-CM4-8}}$ , the three approaches based on quantile mapping (QM, CDF-t, and dOTC) lower the median closer to the  $LG_{\text{CRUJRA}}$  median. For the wet model, all approaches lead to significant improvement compared to the target dataset. None of the arithmetic or weighted ensemble averages in FPC match the  $LG_{\text{CRUJRA}}$  median and are mostly below the lower quartile of  $LG_{\text{CRUJRA}}$ .

Overall, the analysis of FPC highlights important implications for bias correction. The results show that LPJ-GUESS responds very differently to the various bias correction methods because the change in the GCM forcing alters the competitive interactions between vegetation types. Importantly, although the spatial maps show similar agreement in  $C_{\text{Total}}$  between correction methods, the change in FPC implies that the resulting change in carbon is simulated by difference underlying vegetation compositions. We therefore further examine the seasonal cycle of GPP of  $C_4$  grasses in the following as the change was the most different after bias correction.

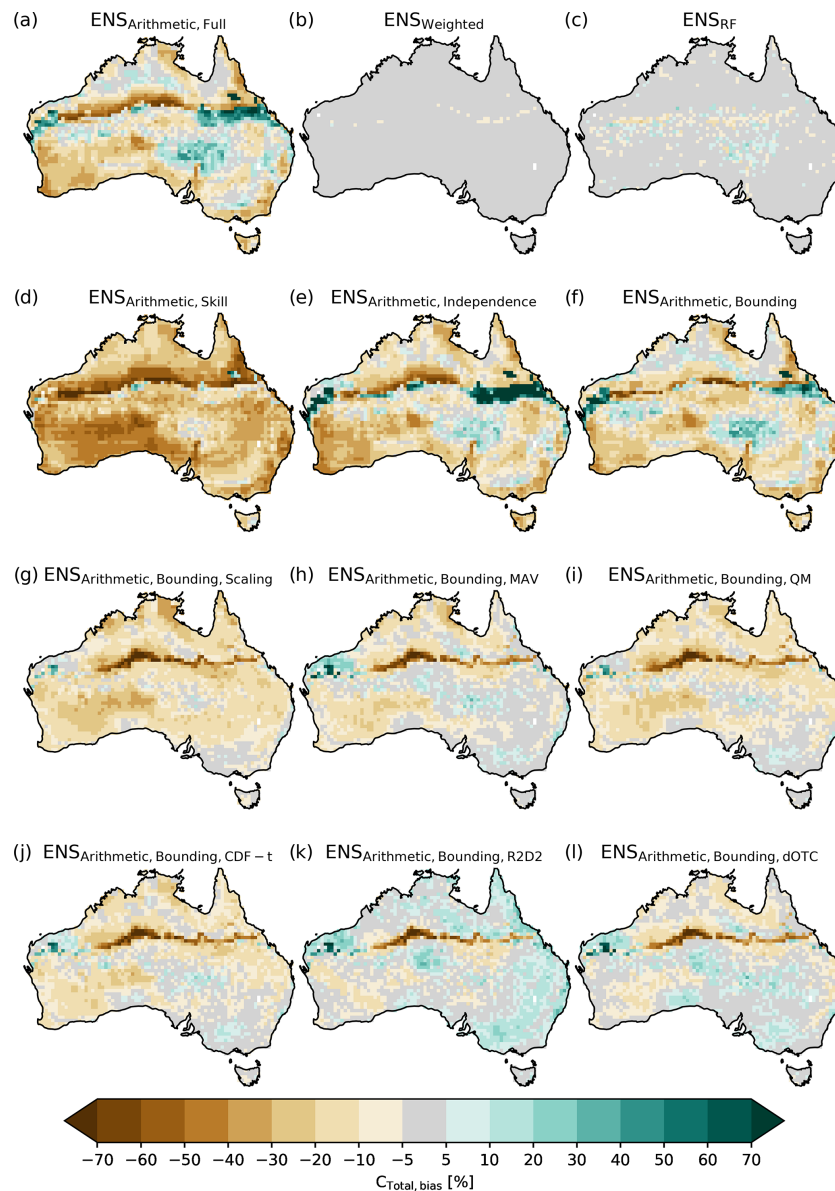


**Figure 5.** Difference between the ensemble averages of  $C_{\text{Total}}$  and  $C_{\text{Total}}$  simulated by  $LG_{\text{CRUJRA}}$ . Panels (a)–(c) show the arithmetic, weighted, and random forest ensemble average based on the LPJ-GUESS runs using the full CMIP6 ensemble, respectively. Panels (d)–(f) show the arithmetic ensemble average based on LPJ-GUESS runs using sub-selections of the CMIP6 ensemble (skilled, independent, and bounding GCMs, respectively). Panels (g)–(l) show the arithmetic ensemble average based on LPJ-GUESS runs using the bias-corrected bounding GCMs following the scaling, MAV, QM, CDF-t, R2D2, and dOTC approach, respectively. The noticeable bias across the Tropic of Capricorn results from the assumed bioclimatic limit for  $C_4$  grasses.

Figure 8 shows the seasonal GPP for  $C_4$  grasses. All simulations, including  $LG_{\text{CRUJRA}}$ , simulate peak productivity in the wet season and minimum productivity in the dry season (see Fig. 8a), but the uncertainty in simulated seasonal GPP is large (see ensemble spread with values between  $\sim 0.1$  and  $0.4 \text{ PgC month}^{-1}$  at the peak of the wet season and  $\sim 0$  and  $0.15 \text{ PgC month}^{-1}$  at the peak of the dry season). Through December to March, the maximum GPP during the wet season is lower compared to the reanalysis results but is closer

to the reanalysis simulations in the dry season. As a result, the bias correction methods achieve similar  $C_{\text{Total}}$  values (see Fig. 3) predominantly through reducing biases during the dry season and introducing an underestimation bias in the wet season. Notably, the R2D2 method always achieves the lowest bias to the target dataset compared to the remaining bias correction methods.

For  $LG_{\text{MPI-ESM2-2-HR}}$ , the raw climate forcing does not generate the right magnitude and timing of peak GPP. When

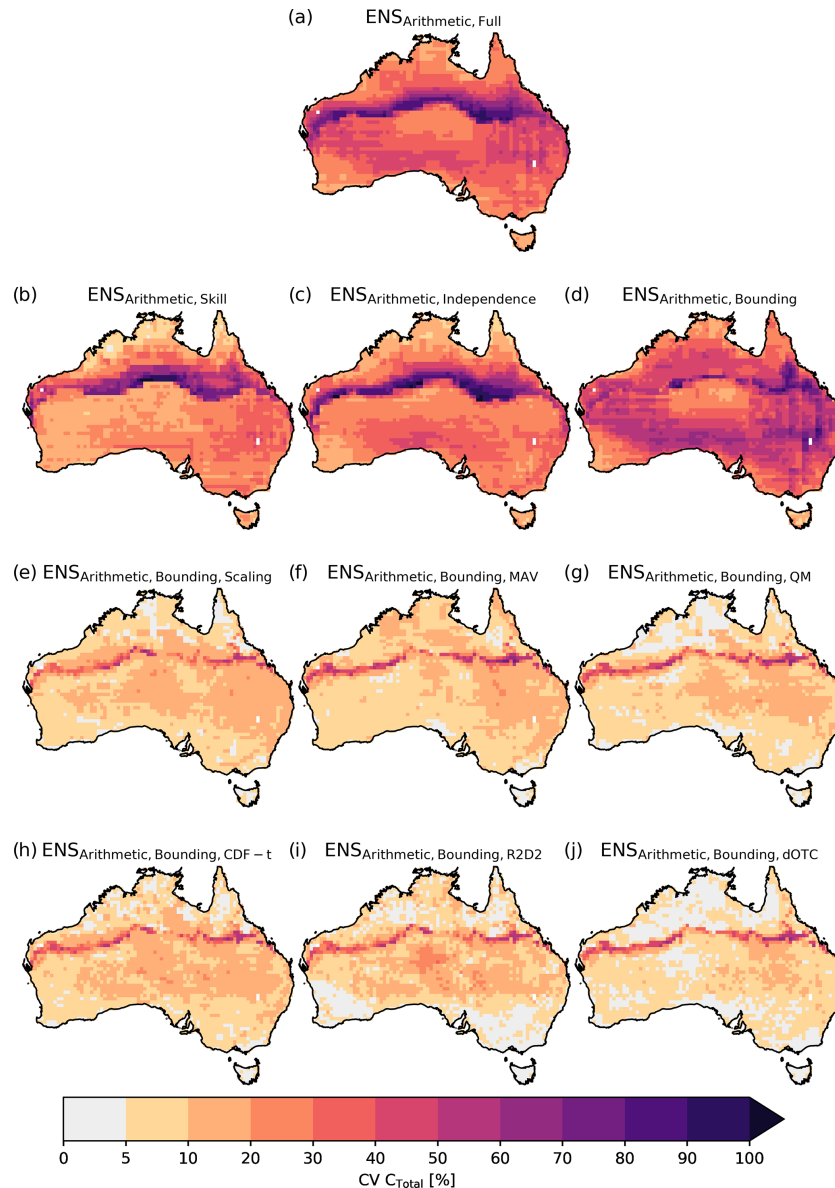


**Figure 6.** Coefficient of variation (CV) over the ensemble of  $C_{\text{Total}}$  simulated by LPJ-GUESS. Panel (a) shows the CV based on the LPJ-GUESS runs using the full CMIP6 ensemble. Panels (d)–(f) show the CV based on LPJ-GUESS runs using sub-selections of the CMIP6 ensemble (skilled, independent, and bounding GCMs, respectively). Panels (g)–(l) show the CV based on LPJ-GUESS runs using the bias-corrected bounding GCMs following the scaling, MAV, QM, CDF-t, R2D2, and dOTC approach, respectively. The noticeable CV across the Tropic of Capricorn results from the assumed bioclimatic limit for  $C_4$  grasses. Note that we do not show a coefficient of variation for the weighted ensemble averages. Given they produce a single estimate rather than an ensemble estimate, a coefficient of variation does not exist for these methods.

corrected with the two multivariate approaches, both become more similar to the LGCRUJRA runs. For LGINM-CM4-8 and LGMPI-ESM1-2-HR, all bias correction methods increase GPP from December to March, while for LGKIOST-ESM only the two multivariate approaches achieve a change closer to the LGCRUJRA runs in the wet season GPP. When the NorESM2-MM climate forcing is corrected, the magnitude is even lower than when the raw climate forcing is used. Figure 8f

also shows the impact of the different ensemble-averaging approaches. Applying the random forest approach leads to near identical result to the LGCRUJRA simulation. Both the weighted and arithmetic ensemble average result in a lower peak in GPP in the wet season, where the arithmetic average is lower than both the random forest result and the weighted average.

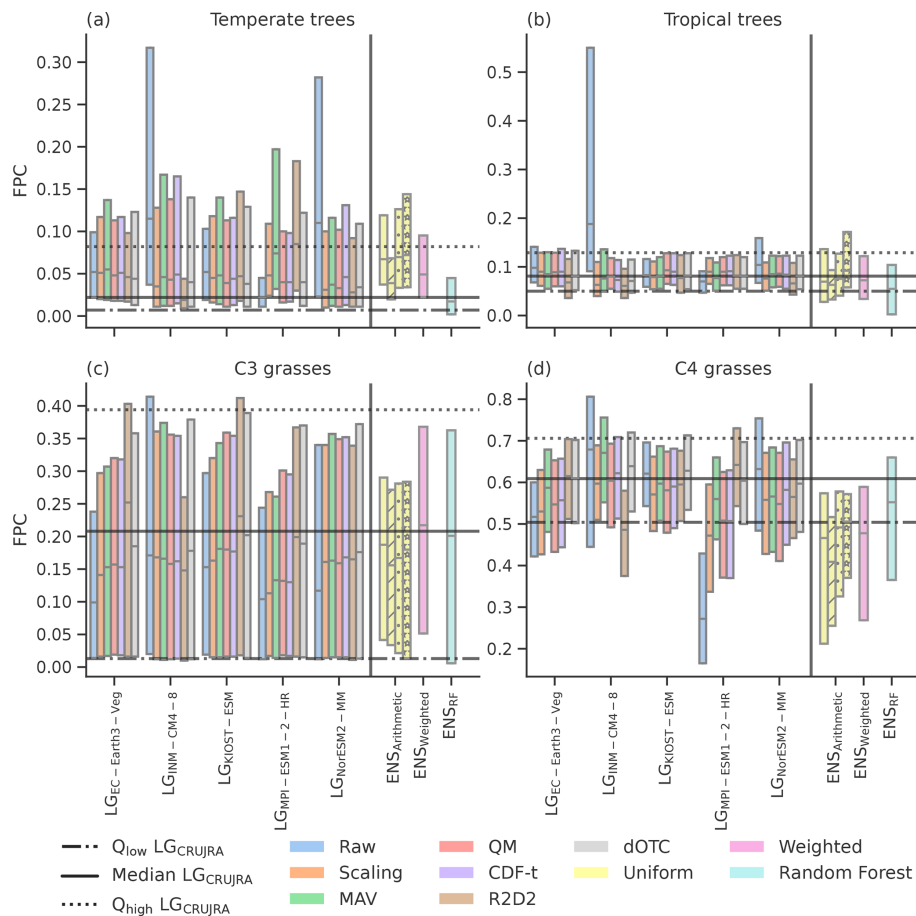


**Figure 7.** Boxplots showing the median, 75th, and 25th percentiles of foliar projective cover (FPC) for temperate (a) and tropical (b) trees and C<sub>3</sub> (c) and C<sub>4</sub> (d) grasses for Australia. The first five groups are the LPJ-GUESS runs based on the five bounding models LG<sub>EC</sub>-Earth3-Veg, LG<sub>INM</sub>-CM4-8, LG<sub>KIOST</sub>-ESM, LG<sub>MPI</sub>-ESM1-2-HR, and LG<sub>NorESM2</sub>-MM, where blue shows the FPC based on the raw model forcing and orange, green, red, purple, brown, and grey show the FPC when LPJ-GUESS is forced with the corrected model forcing following the scaling, MAV, QM, CDF-t, dOTC, and R2D2 method, respectively. The yellow, pink, and bright blue boxplots on the right-hand side of each panel show the different ensemble-averaging methods (arithmetic average, weighted average, and random forest, respectively) when the full ensemble is used (group “full”). The groups “skill” (dashed), “independence” (dotted), and “bounding” (filled with stars) show the results for the arithmetic average when only a sub-selection of models is used (see Sect. 3.1). The solid lines show the median values of the simulations with the CRUJRA reanalysis, the dotted lines are the 75th percentile, and the dashed–dotted line is the 25th percentile.

## 5 Discussion

In this study, we explored the impact of climate model uncertainty on the regional carbon cycle over Australia and the sensitivity of the carbon cycle to different approaches to correcting climate forcing biases. We found that, uncorrected, the continental-scale climate projections over Australia were associated with large uncertainties. The difference between the hottest and coldest model is very large, 3.4 °C higher than the observed historical warming over the continent (1.4 °C; IPCC, 2021), and local differences can be even larger. Similarly, average precipitation ranges between 254 and 858 mm yr<sup>-1</sup>, and the IAV ranges from 55 to 183 mm yr<sup>-1</sup>. The differences on both timescales have a large impact on predicted vegetation, especially across a

water-limited continent such as Australia. Our finding that the simulation of Australia’s carbon cycle is particularly sensitive to the choice of climate forcing is consistent with previous studies (e.g., Ahlström et al., 2012, 2015, 2017). The uncertainty in the CMIP6 forcing translates into a significant variability in the simulated carbon cycle in LPJ-GUESS; for example, the average values for  $C_{\text{Total}}$  vary between 28.6 and 75.1 PgC, and the IAV in NBP was between 0.3 and 1.1 PgC. We explored three approaches to reduce biases and ensemble uncertainty and discuss each in turn below.

### 5.1 Sensitivity to bias correction methods

We tested six different methods for bias-correcting the CMIP model forcing driving LPJ-GUESS. Four methods incorpo-

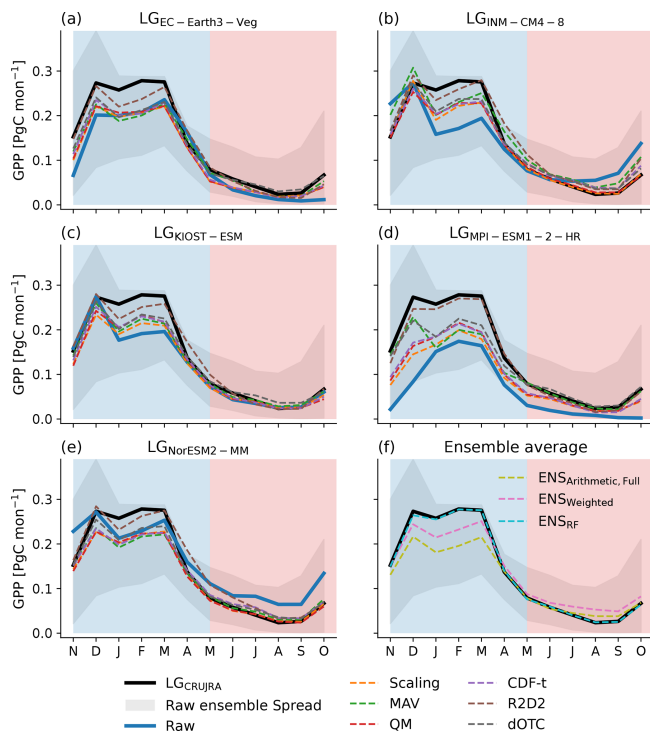


**Figure 8.** Seasonal cycle of gross primary productivity for  $C_4$  grasses in Australia. The different panels show the seasonality when LPJ-GUESS is forced with the bounding five bounding models (a–e). The different colors show the unconstrained model climate forcing (blue) or after bias-correcting the data following the scaling (orange), mean and variance (green), quantile mapping (red), CDF-t (purple), dOTC (brown), and R2D2 (grey) methods. The black lines represent the reanalysis simulations with CRUJRA, and the grey shading shows the full CMIP6 ensemble spread. The blue-shaded area indicates the wet season (November–April), and the red-shaded area shows the dry season (May–October).

rate univariate approaches (each climate variable is corrected independently), while the remaining two employ multivariate approaches (inter-variable relationships are accounted for). The methods tested range in complexity. The widely used scaling method applied in this study can correct the mean values of the variables; however, it cannot adjust variability and extreme values correctly (see, for example, Berg et al., 2012). The mean and variance approach therefore builds on the scaling method by correcting both mean and variance. We also considered two alternative approaches that attempt to correct the bias based on their distribution, i.e., quantile mapping and CDF-t. The basic quantile mapping method not only corrects the mean bias but also adjusts the distribution and may therefore be more suitable when both the average and extremes are studied. Based on quantile mapping, the CDF-t method additionally incorporates projected changes in mean and variability simulated by the GCM. In contrast to the univariate approaches discussed, multivariate correction methods allow us to adjust inter-variable dependencies. One of the main dif-

ferences between the dOTC and R2D2 methods applied here is that dOTC is designed to transfer some of the multidimensional properties from the GCM to the bias-corrected data (such as the change in time; see François et al., 2020). The R2D2 approach instead assumes that inter-variable and inter-site rank correlations are stable in time.

We found that all bias correction methods reduce the average bias of  $C_{\text{Total}}$  to that of the reference run for the five individual models. When deriving an arithmetic ensemble average of the raw and bias-corrected results, the values for the ensemble averages are relatively similar. Correcting the climate forcing significantly reduces the spread amongst the ensemble members compared to the raw model forcing. We further explored regional differences for Australia in the  $C_{\text{Total}}$  bias compared to our reference run and found that all bias correction methods reduce the magnitude of the bias. The spatial patterns in bias were consistent across the bias correction methods, implying that the relative spatial distribution of  $C_{\text{Total}}$  remains similar. We note that all maps display high values for both bias and CV in  $C_{\text{Total}}$  across the Tropic of Capricorn ( $23^{\circ}26'10.7''$  S). This is an artifact resulting from assumed model bioclimatic limits. In LPJ-GUESS, vegetation growth of  $C_4$  grasses and tropical trees is restricted by a lower temperature boundary such that these vegetation types cannot establish or survive when the 20-year-average minimum temperature falls below  $15.5^{\circ}\text{C}$ . Therefore,  $C_4$  grasses and tropical trees only grow north of the Tropic of Capricorn, while south of it only temperate trees and  $C_3$  grasses are simulated. The strong variation across GCMs in simulated temperature thus leads to very different simulated vegetation cover (and thus high CV) in LPJ-GUESS.

In contrast to the average  $C_{\text{Total}}$  results, bias-correcting the forcing CMIP models does not necessarily lead to better results for other variables simulated by LPJ-GUESS. The different bias correction approaches did not necessarily lead to improved simulations of the change in  $C_{\text{Total}}$  compared to the target dataset. The arithmetic average across all five bounding models is relatively close to that of the reference run, and the upper boundary of the model spread was reduced when bias correction methods were applied. However, the lower boundary was almost the same or slightly worse than before (EC-Earth3-Veg). The different biases and magnitudes in  $C_{\text{Total}}$  reflect that the underlying vegetation composition may vary depending on the CMIP6 ensemble member used to run LPJ-GUESS and the bias correction method.

The foliar projective cover gives an indication of the fidelity of vegetation cover. In LPJ-GUESS, FPC results from simulated vegetation competition, which in turn is influenced by the climate input forcing. For example, water-limited regions such as arid Australia will have limited tree growth and increased grass growth. Further, competitive processes amongst tree species and  $C_3$  and  $C_4$  grasses that are driven by temperature (either dynamically or prescribed) can drive vegetation competition and therefore FPC. We found that temperate trees and  $C_4$  grasses in particular can vary strongly in



dominance and relative cover depending on the GCM used as the input forcing and the bias correction applied. Only the two multivariate approaches adjust the distribution so that it is more comparable to the reference dataset and the other ensemble members. This implies that both the model selection and the bias correction method can lead to small but potentially important differences in composition of vegetation distributions across the landscape. Models that show large differences in the vegetation distribution are also sensitive to the bias correction for seasonal GPP. For the two models with the strongest divergence in  $C_4$  grass distribution, all bias correction methods improve the seasonal productivity compared to the target dataset. However, correcting the climate forcing also led to a lower skill in predicting seasonal GPP for one model (LG<sub>NorESM2-MM</sub>). We also found the foliar projective cover, especially that of  $C_4$  grasses, showed a strong sensitivity to the bias correction method chosen for some models (e.g., MPI-ESM1-2-HR). However, the spatial patterns in average bias of  $C_{\text{Total}}$  remain relatively consistent across all bias correction methods tested and show some similarity to that of the raw model forcing (LG<sub>EC-Earth3-Veg</sub>, LG<sub>KIOST-ESM</sub>, and LG<sub>NorESM2-MM</sub>). This outcome may emerge as we corrected each grid cell independently. When François et al. (2020) correct their climate variables taking into account spatial properties, both methods tested here improved the results for small regional scales. Given the heterogeneity of climate and large area of the Australian continent, we did not attempt to correct the spatial scales given limitations in computation time, but this would be worth exploring in future work.

In summary, within a framework of testing bias correction methods on the five models spanning the CMIP6 model spread, we found that the bias correction methods successfully reduced the bias to the reference dataset for averages over time and space ( $C_{\text{Total}}$ ). Overall, the two multivariate approaches achieved a stronger reduction in bias for both individual GCMs and the ensemble average while also presenting a lower uncertainty across the ensemble. A clear advantage of applying multivariate approaches is that they account for inter-variable dependencies and can therefore preserve the consistency between the climate variables used to drive LPJ-GUESS. However, the variation across the different correction methods is small, and value ranges for multivariate approaches are comparable to the univariate quantile mapping approaches. Given the increased computation cost associated with multivariate approaches and the limited benefit demonstrated in this study, multivariate bias correction methods may therefore not necessarily be the best approach in future impact studies. Further, all correction methods show limited impact for other temporal properties (such as the change over time; e.g., Hagemann et al., 2011; Maurer and Pierce, 2014; Cannon et al., 2015; François et al., 2020). For example, Hagemann et al. (2011) found that bias correction does not necessarily lead to a more realistic climate change signal. In a different study focusing on precipitation, Maurer and Pierce (2014) demonstrated that long-term changes in simu-

lated precipitation can artificially deteriorate following quantile mapping. Further, Cannon et al. (2015) find that quantile mapping approaches can inflate relative trends in precipitation extremes projected by GCMs. The lack of skill in correcting temporal properties was also demonstrated for multivariate bias correction approaches (François et al., 2020). Using single models or even a subset of the ensemble may therefore not inform trends and processes on short timescales for studies exploring the future carbon cycle. Conversely, explicitly bias-correcting trends based on historical data, when the spatiotemporal nature may not yet have clearly emerged, could equally be problematic for unbiased estimation of climate system properties like equilibrium climate sensitivity. Despite the demonstrated limited impact of bias correction on temporal and spatial scales, correcting the driving forcing is still preferable to using raw climate forcing. DGVMs largely rely on bioclimatic limits that define where specific types of vegetation can grow. Relying on a biased climate forcing dataset might therefore result in a misrepresentation of the vegetation. Indeed, we found strong differences in the foliar projective cover of different vegetation groups. This mismatch in vegetation composition that can result from threshold-defined boundaries is likely to lead to diverging carbon and water cycle responses to the climate, which might be even more pronounced in areas with higher vegetation carbon mass than Australia. Future studies could further explore options to improve temporal features in climate variables. Robin and Vrac (2021), for example, include time as an additional variable for their multivariate bias correction, which may be a promising avenue for future research.

Climate change impact studies need to be aware of the limitations of bias correction methods. As we have shown, bias correction cannot solve fundamental deficiencies in GCMs (Maraun et al., 2017). A possible flaw in applying univariate bias correction methods to a set of climate variables needed to force a dynamic vegetation model is a resulting inconsistency within the climate forcing. While all bias correction methods improve the averages of  $C_{\text{Total}}$  compared to the target dataset, importantly, based on our findings it is not clear that one method systematically outperforms any other. This may be because the carbon cycle in Australia is mostly driven by precipitation, and for vegetation limited by both temperature and precipitation, multivariate approaches may outperform univariate approaches more distinctly (Zscheischler et al., 2019). While the ensemble average is mostly insensitive to the choice of raw or corrected data, the spread between the outlier models is significantly reduced by any of the correction methods (especially the quantile mapping approaches and the multivariate dOTC method). Other temporal properties, such as the change over time, are not necessarily improved or can even deteriorate compared to the raw climate forcing, such as the trend, interannual variability or extreme events. Researchers should be especially cautious when they rely on a small sub-sample or even single models for their impact study, given different GCMs can react differently to

the same bias correction method (e.g., for  $LG_{INM-CM4-8}$ , the magnitude in bias is reduced, while for  $LG_{NorESM2-MM}$  the sign in bias can change depending on correction method applied).

## 5.2 Sensitivity to ensemble-averaging methods and model selection methods

We also tested the commonly used arithmetic ensemble average, a weighted averaging approach following Bishop and Abramowitz (2013), and a random forest regression approach. We found that the weighted average and the random forest approach outperform the arithmetic ensemble average for average  $C_{Total}$ , and seasonal GPP with results very similar to the reference dataset. The random forest approach produces a small error magnitude when spatial dimensions are explored (see Fig. 5) while for the arithmetic and weighted ensemble average, systematic biases persist. While the FPC of tropical trees and  $C_3$  grasses seems to be broadly captured by all averaging methods,  $C_4$  grasses shows a strong bias where only the random forest approach achieves a median value within the IQR of the  $LG_{CRUJRA}$  run. As shown in previous studies (e.g., Bishop and Abramowitz, 2013; Knutti et al., 2017; Abramowitz et al., 2019; Merrifield et al., 2020) there is benefit to avoiding the use of the arithmetic ensemble-averaging method for impact studies. An additional caveat of the arithmetic ensemble average is the sensitivity to the model selection. The ensemble average somewhat depends on the models it is derived from. Counterintuitively, choosing the models that show high skill in simulating precipitation led to the worst results in most cases (a result similar to Herger et al., 2018).

## 5.3 General caveats

All methods explored in this study rely on the general assumption that the reanalyses used to describe the historical time period are accurate and that the methods employed apply equally to the past and the future. It seems reasonable to argue that methods that fail to constrain models in the historical period are unlikely to work well for future periods. Unfortunately, the converse point that methods that work well in the historical period will necessarily work well in the future is not always true. Shifts in atmospheric circulation, emergence of novel climates, or the triggering of ecosystem tipping points might alter land–atmosphere feedbacks that lead to changes in the climate such that methods that are reliable in the historical period cease to be reliable in the future.

A possible caveat in our study setup is the design of the ensemble subsets. We selected all models based on the simulated precipitation based on the assumption that precipitation is the most important driver of Australia's carbon cycle. However, temperature and perhaps the extremes of temperature may also be an important constraint for vegetation distribution (especially in LPJ-GUESS where vegetation grows

within predefined bioclimatic limits that are based on temperature like the boundary between  $C_3$  and  $C_4$  grasses). However, when we repeated the analysis using the raw temperature and incoming shortwave radiation forcing and bias-corrected precipitation data, the results were almost identical compared to the runs where all climate variables were corrected, confirming that precipitation drives the carbon cycle response within this framework. Further, for simulating vegetation the skill of the variables may be important on multiple timescales. We attempt to account for this in the model selection methods by applying the respective metrics on monthly and annual timescales. In addition, the response of the simulated terrestrial carbon cycle to the climate forcing is intimately linked to the sensitivity to the atmospheric  $CO_2$  concentration. This study chose a model setup with both transient atmospheric  $CO_2$  concentration and nitrogen deposition, and therefore it does not fully isolate the impact of the climate forcing. However, given all LPJ-GUESS simulations have the same configuration apart from the climate forcing, i.e., the prescribed atmospheric  $CO_2$  concentration and nitrogen deposition are identical, we argue that our experiment setup is suitable for this study. Lastly, five models for all selection methods may seem like a small subset. However, earlier studies (e.g., Pierce et al., 2009) found that the multi-model ensemble mean tends to converge towards a similar value after including five models. We therefore conclude that five models was a sufficient number in our testing framework.

We further chose a relatively short calibration time period (1989–2010) to allow sensitivity tests with multiple reanalysis datasets. While these 22 years may not cover decadal variability, we assume it is sufficient to account for interannual variability such as the El Niño–Southern Oscillation, the Indian Ocean Dipole, and Southern Annular Mode, which have been shown to be important influences on the Australian carbon cycle (e.g., Cleverly et al., 2016).

Other areas of uncertainty may include the sensitivity of the methods to the reference dataset. Several studies have discussed that both bias correction methods (e.g., Iizumi et al., 2017; Famien et al., 2018; Casanueva et al., 2020) and weighted ensemble-averaging methods (e.g., Merrifield et al., 2020) depend on the observation dataset they are calibrated on. Casanueva et al. (2020) demonstrate that precipitation in particular is sensitive to the choice of reference dataset. We therefore repeated the bias correction and chose ERA5 as a second dataset. We found high correlation coefficients between LPJ-GUESS runs that are based on GCMs corrected to CRUJRA and LPJ-GUESS runs that were based on GCMs corrected to ERA5 for  $C_{Total}$  (0.96–0.98; not shown here). We conclude that our results were robust to the choice of reference dataset. Another concern frequently discussed is impact of the mismatch in spatial resolution (high-resolution reanalysis product vs. low-resolution GCM output). A solution to reduce the mismatch in spatial resolution might be to use dynamically downscaled datasets such as

CORDEX. However, Casanueva et al. (2020) find the impact of the horizontal resolution on the bias correction results to be small in comparison to the impact of the bias correction method. Given dynamically downscaled products were only available for older CMIP generations (CORDEX is based on CMIP5, while NarCLIM is based on CMIP3) or contained only a small subset of GCMs (ISIMIP), and we expected the uncertainty associated with the spatial mismatch to be small, we chose the state-of-the-art CMIP6 GCM output.

Further, in this study, we chose just one realization from each GCM, and therefore the results presented in this study do not fully reflect the uncertainty in simulations of the terrestrial carbon cycle linked to the entire spectrum of possible GCM forcings. Adding more realizations would significantly increase the computational costs, and we do not expect that our results would differ significantly. Ukkola et al. (2020) looked at the effects of additional ensemble members in their assessment of future rainfall change and found limited sensitivity. Nevertheless, to fully understand the impact of uncertainty in simulated climate within individual GCMs, future work could consider using the CESM large ensemble. In addition, Teckentrup et al. (2021) showed significant uncertainty in the simulated terrestrial carbon cycle linked to the choice of DGVM, but in this study we chose a single DGVM to study the impact of climate uncertainty. However, to capture the full uncertainty and to achieve a stronger constraint on the simulated terrestrial carbon cycle, future work could explore the response in other members of the TRENDY ensemble and create an ensemble composed of both different DGVMs and different GCM climate forcings.

Lastly, we chose to correct daily climate data for the main analysis. However, correcting monthly data may be statistically more robust, especially for highly variable climate variables with a large number of null values such as daily precipitation. Indeed, our analysis of the corrected input variables surprisingly showed an increase in bias in simulated precipitation for two GCMs after correction (see Fig. 3) that is likely linked to a mismatch in simulated days without rain in the target dataset and the GCM simulation. We additionally tested the importance of timescales; i.e., we bias-corrected the GCMs on both daily and monthly timescales before forcing LPJ-GUESS with them.  $C_{\text{Total}}$  simulated by LPJ-GUESS driven by daily and monthly corrected GCM output was strongly correlated (0.92–0.99; not shown here). Given only a few grid cells displayed an unreasonably high bias in precipitation (not shown) and the fact that vegetation growth is also driven by temperature and incoming shortwave radiation in LPJ-GUESS, we assume that the impact on the simulated carbon on monthly to multidecadal timescales is small.

#### 5.4 Implications

Based on our findings, we conclude that decisions in regard to model selection, bias correction of GCM output,

and ensemble-averaging methods, may alter future projections of ecosystem studies, especially the uncertainty estimates. Selecting a subset of models to reduce computation time is common, but sensitive to the criterion chosen for both arithmetic average and uncertainty estimate. While choosing GCMs based on how well they represent the historical climate may seem intuitive, we find that the arithmetic average based on a subset representing only independent models or models that define the full ensemble spread reduces the bias compared to our reference run. Conversely, a subset of only skilled models reduces the ensemble uncertainty. However, this reduction in uncertainty may stem from the wrong biophysical reasons, and a sub-selection of skilled models might not truly represent all plausible GCM outputs.

We further demonstrate that correcting GCM output can significantly alter Australia's carbon cycle projections. Bias corrections, however, only reduce the biases in relatively steady vegetation variables, such as the longer-term carbon states. Averaged over the continent, we find that LPJ-GUESS forced with individually corrected GCM output can be sensitive to the bias correction method, but the arithmetic ensemble averages were found to be insensitive. Some bias correction methods did reduce the ensemble uncertainty more than others (e.g., scaling vs. dOTC). On smaller scales, i.e., exploring regional differences or on PFT level, the choice of bias correction method can have a big influence on species distribution and magnitude in fluxes. Correcting biases may also lead to different outcomes relying on thresholds of absolute values when applied to individual GCMs, such as for climate threshold studies exploring tipping points.

Importantly, bias correction methods do not correct temporal (such as IAV or trend) and spatial properties unless the methods are specifically designed and set up to do so. We found that using corrected GCM output can even increase the distance in change compared to our reference dataset. Future studies of ecosystem and carbon cycle impacts based on GCM climate forcing should therefore carefully choose a subset of models that is representative of the ensemble uncertainty and not rely on using a single GCM.

To conclude, when Pandora opened the lid on her box she released the evils of the world, and these could never be put back into the box. We fear that we have also made the challenge of constraining the future regional-scale carbon budgets more difficult. We have, for example, raised more questions than answers, identified limitations of existing approaches, and ultimately provided a challenge to the community to find more robust strategies to reduce the uncertainty in the projection of regional carbon stores. We acknowledge we have not provided easy answers, but we hope that by highlighting the challenges, strategies may be developed that can robustly constrain regional estimates of carbon storage.

Appendix A

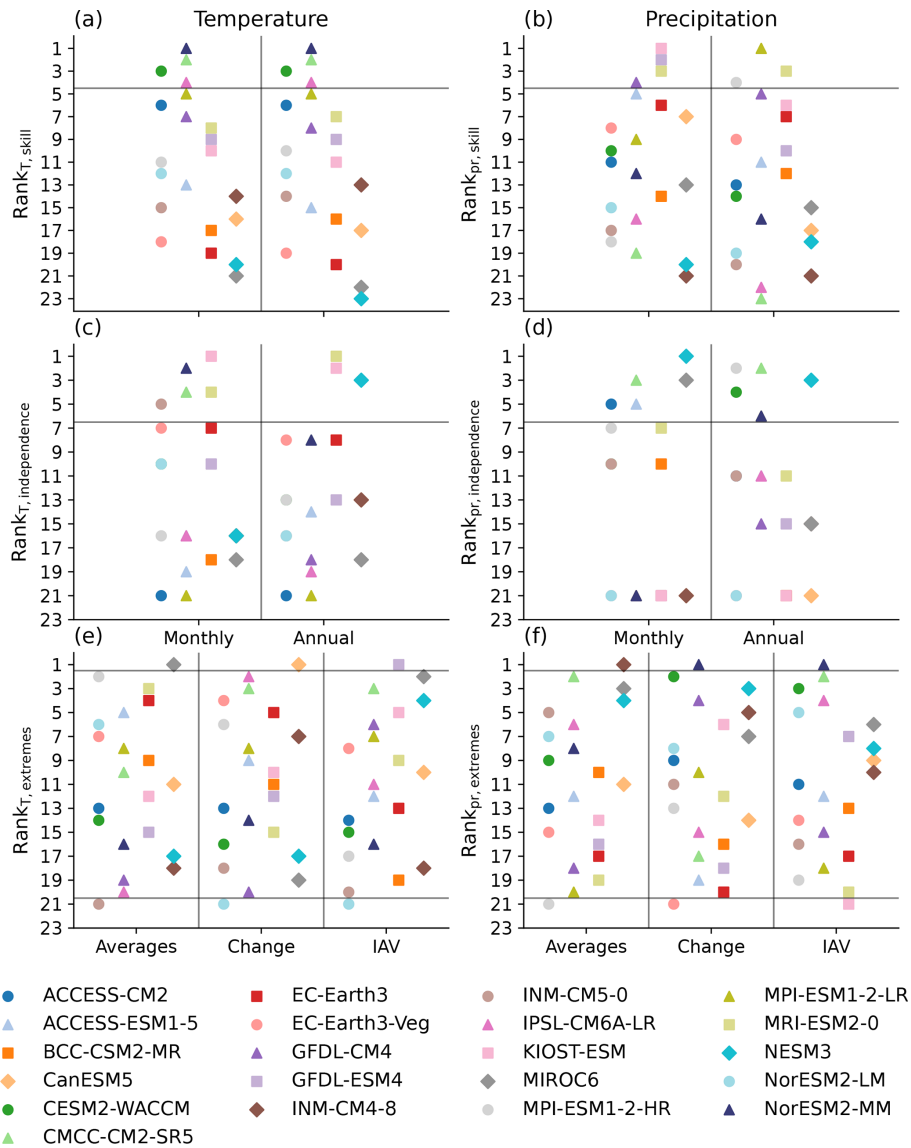


**Figure A1.** Ranks derived for CMIP6 GCM sub-selection. Panels (a) and (b) show the rank according to the skill of each GCM in simulating temperature (a) and precipitation (b) on monthly and annual timescales for Australia (compare Table 2 and Sect. 3.1.1). Panels (c) and (d) show the independence rank of each GCM for temperature (c) and precipitation (d) on monthly and annual timescales (compare Sect. 3.1.2). Lastly, (e) and (f) show the GCMs defining the ensemble spread, i.e., the GCM simulating the highest and lowest total amount in precipitation (“averages”), change in precipitation (“change”), and interannual variability (“IAV”; compare Sect. 3.1.3).

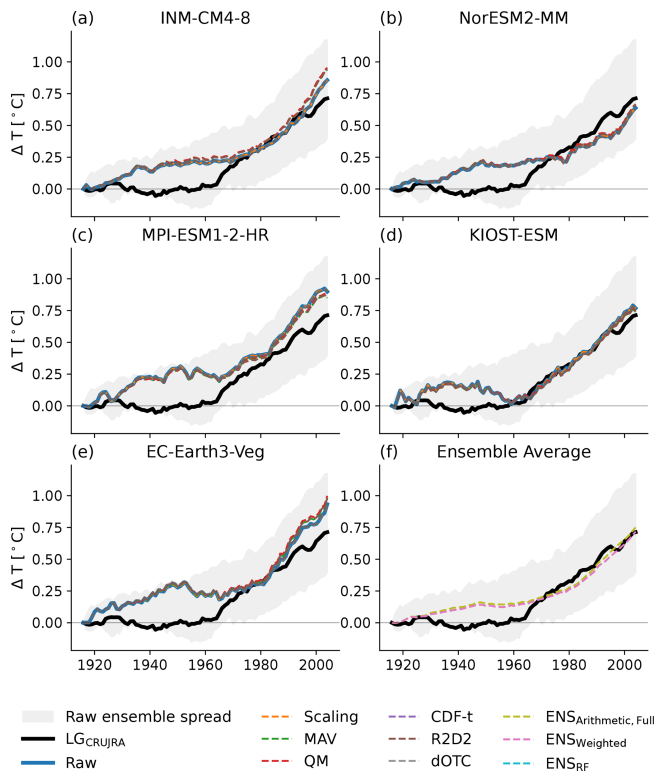


**Figure A2.** The 30-year moving average of the change in temperature ( $T$ ) averaged over Australia. In each panel, the bold black line is the change in  $T$  based on the CRUJRA reanalysis, while the grey-shaded area represents the full unconstrained CMIP6 model ensemble. Panels (a)–(e) show the  $T$  change based on the five bounding models. The colors show the change in  $T$  based on the different bias correction methods. Panel (f) shows the change in  $T$  estimated by the ensemble-averaging methods.

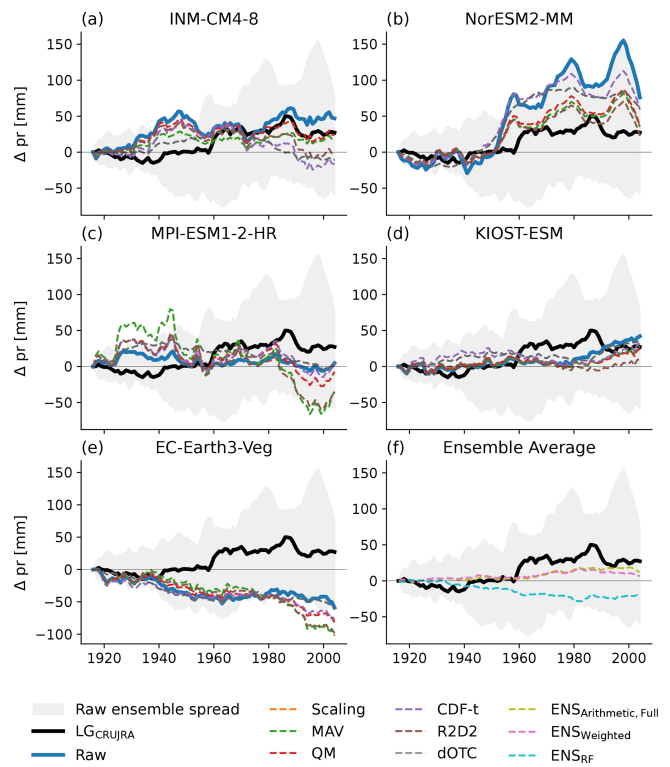


**Figure A3.** The 30-year moving average of the change in precipitation (pr) averaged over Australia. In each panel, the bold black line is the change in pr based on the CRUJRA reanalysis, while the grey-shaded area represents the full unconstrained CMIP6 model ensemble. Panels (a)–(e) show the pr change based on the five bounding models. The colors show the change in pr based on the different bias correction methods. Panel (f) shows the change in pr estimated by the ensemble-averaging methods.

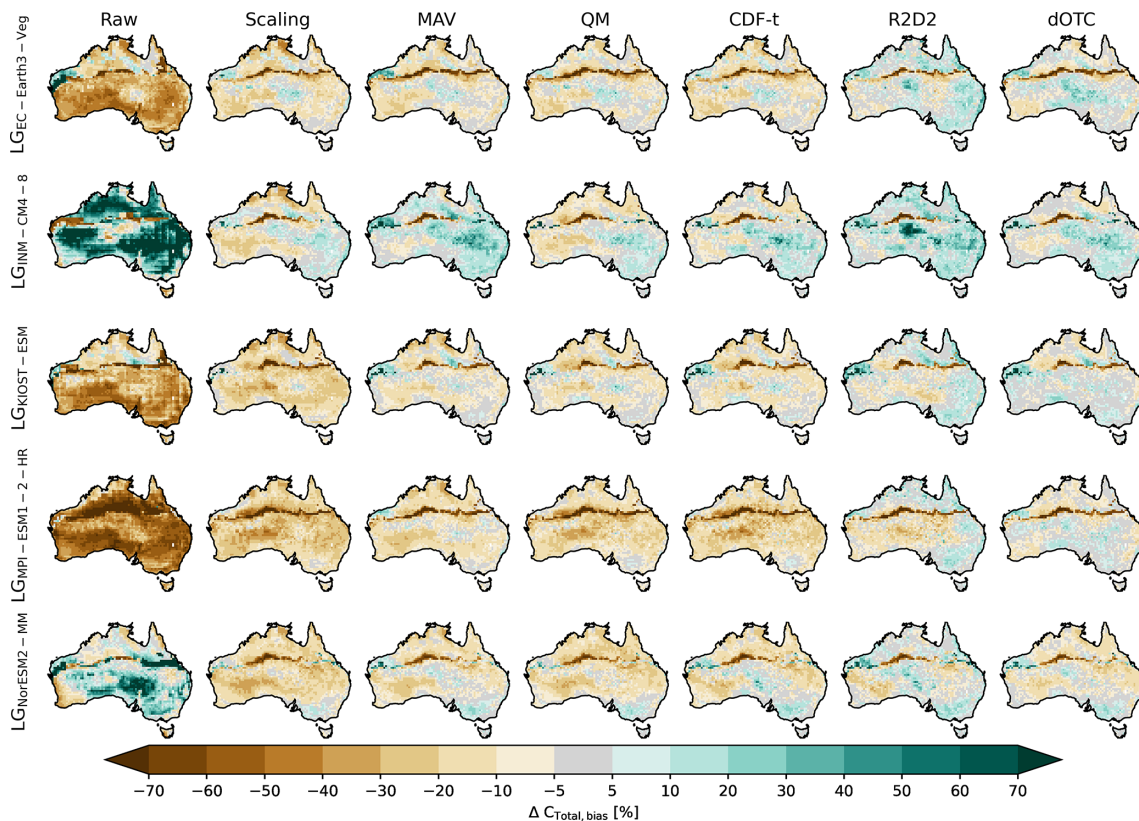


**Figure A4.** Difference between the simulated  $C_{\text{Total}}$  based on the five bounding models and the CRUJRA reanalysis when LPJ-GUESS is forced with the raw model forcing or with the corrected forcing following the scaling, MAV, QM, CDF-t, dOTC, and R2D2 approach. The bottom row shows the different ensemble-averaging methods (arithmetic average, weighted average, and random forest).

**Code and data availability.** The CMIP6 output used in this study is available via the Earth System Grid Federation (ESGF, 2023, <https://esgf-node.llnl.gov/search/cmip6/>). The CRUJRA reanalysis dataset is accessible via <https://catalogue.ceda.ac.uk/uuid/7f785c0e80aa4df2b39d068ce7351bbb> (Harris, 2019). The bias correction is applied based on the Python SBCK package <https://github.com/yrobink/SBCK> (Robin, 2022). The analysis code can be found at <https://doi.org/10.5281/zenodo.7882380> (Teckentrup, 2023).

**Author contributions.** LT, MGDK, and AJP designed and conducted the experimental analysis. LT, MGDK, AJP, and GA wrote the first draft with contributions from AMU, SH, BS, and BF. AMU preprocessed the CMIP6 GCM output. BF helped to implement the bias correction methods. GA and SH developed the weighted ensemble-averaging method. All authors contributed to the final manuscript. Correspondence and requests for materials should be addressed to LT ([l.teckentrup@westernsydney.edu.au](mailto:l.teckentrup@westernsydney.edu.au)).

**Competing interests.** The contact author has declared that none of the authors has any competing interests.

**Disclaimer.** Publisher's note: Copernicus Publications remains neutral with regard to jurisdictional claims in published maps and institutional affiliations.

**Acknowledgements.** We are grateful to the National Computational Infrastructure at the Australian National University for the provision of supercomputing resources.

**Financial support.** The research was funded by the ARC Centre of Excellence for Climate Extremes (CE170100023) and by the New South Wales Department of Planning, Industry and Environment. Martin G. De Kauwe and Andrew J. Pitman received support from the ARC Discovery Grant (DP190101823). Martin G. De Kauwe received support from the NSW Research Attraction and Acceleration Program (RAAP). Anna M. Ukkola received support from the Australian Research Council (DE200100086).

**Review statement.** This paper was edited by Anping Chen and reviewed by Alexander J. Winkler and two anonymous referees.

## References

- Abramowitz, G., Herger, N., Gutmann, E., Hammerling, D., Knutti, R., Leduc, M., Lorenz, R., Pincus, R., and Schmidt, G. A.: ESD Reviews: Model dependence in multi-model climate ensembles: weighting, sub-selection and out-of-sample testing, *Earth Syst. Dynam.*, 10, 91–105, <https://doi.org/10.5194/esd-10-91-2019>, 2019.
- Ahlström, A., Schurgers, G., Arneth, A., and Smith, B.: Robustness and uncertainty in terrestrial ecosystem carbon response to CMIP5 climate change projections, *Environ. Res. Lett.*, 7, 044008, <https://doi.org/10.1088/1748-9326/7/4/044008>, 2012.
- Ahlström, A., Raupach, M. R., Schurgers, G., Smith, B., Arneth, A., Jung, M., Reichstein, M., Canadell, J. G., Friedlingstein, P., Jain, A. K., Kato, E., Poulter, B., Sitch, S., Stocker, B. D., Viomy, N., Wang, Y. P., Wiltshire, A., Zaehle, S., and Zeng, N.: The dominant role of semi-arid ecosystems in the trend and variability of the land CO<sub>2</sub> sink, *Science*, 348, 895–899, <https://doi.org/10.1126/science.aaa1668>, 2015.
- Ahlström, A., Schurgers, G., and Smith, B.: The large influence of climate model bias on terrestrial carbon cycle simulations, *Environ. Res. Lett.*, 12, 014004, <https://doi.org/10.1088/1748-9326/12/1/014004>, 2017.
- Annan, J. D. and Hargreaves, J. C.: On the meaning of independence in climate science, *Earth Syst. Dynam.*, 8, 211–224, <https://doi.org/10.5194/esd-8-211-2017>, 2017.
- Bárdossy, A. and Pegram, G.: Multiscale spatial recorelation of RCM precipitation to produce unbiased climate change scenarios over large areas and small, *Water Resour. Res.*, 48, W09502, <https://doi.org/10.1029/2011WR011524>, 2012.
- Berg, P., Feldmann, H., and Panitz, H.-J.: Bias correction of high resolution regional climate model data, *J. Hydrol.*, 448–449, 80–92, <https://doi.org/10.1016/j.jhydrol.2012.04.026>, 2012.
- Bi, D., Dix, M. R., Marsland, S. J., Farrell, S. P. O., Rashid, H. A., Uotila, P., Hirst, A. C., Kowalczyk, E. A., Golebiewski, M., Sullivan, A., Yan, H., Hannah, N., Franklin, C., Sun, Z., Vohralik, P. F., Watterson, I. G., Zhou, X., Fiedler, R. A. S., Collier, M. A., Ma, Y., Noonan, J. A., Stevens, L., Uhe, P., Zhu, H., Griffies, S. M., Hill, R., Harris, C., and Puri, K.: The ACCESS coupled model: description, control climate and evaluation, *Aust. Meteorol. Ocean.*, 63, 41–64, 2013.
- Bishop, C. and Abramowitz, G.: Climate Model Dependence and the Replicate Earth Paradigm, *Clim. Dynam.*, 41, 885–900, <https://doi.org/10.1007/s00382-012-1610-y>, 2013.
- Boe, J.: Interdependency in multimodel climate projections: Component replication and result similarity, *Geophys. Res. Lett.*, 45, 2771–2779, 2018.
- Boucher, O., Servonnat, J., Albright, A. L., Aumont, O., Balkanski, Y., Bastrikov, V., Bekki, S., Bonnet, R., Bony, S., Bopp, L., Braconnot, P., Brockmann, P. and Cadule, P., Caubel, A., Cheruy, F., Codron, F., Cozic, A., Cugnet, D., D'Andrea, F., Davini, P., de Lavergne, C., Denvil, S., Deshayes, J., Devillers, M., Ducharne, A., Dufresne, J.-L., Dupont, E., Éthé, C., Fairhead, L., Falletti, L., Flavoni, S., Foujols, M.-A., Gardoll, S., Gastineau, G., Ghattas, J., Grandpeix, J.-Y., Guenet, B., Guez, L., E., Guilyardi, E., Guimberteau, M., Hauglustaine, D., Hourdin, F., Idelkadi, A., Joussaume, S., Kageyama, M., Khodri, M., Krinner, G., Lebas, N., Levassieur, G., Lévy, C., Li, L., Lott, F., Lurton, T., Luysaert, S., Madec, G., Madeleine, J., Maignan, F., Marchand, M., Marti, O., Mellul, L., Meurdesoif, Y., Mignot, J., Musat, I., Otlé, C., Peylin, P., Planton, Y., Polcher, J., Rio, C., Rochetin, N., Rousset, C., Sepulchre, P., Sima, A., Swingedouw, D., Thiéblemont, R., Traore, A. K., Vancoppenolle, M., Vial, J., Vialard, J., Viomy, N., and Vuichard, N.: Presentation and Evaluation of the IPSL-CM6A-LR Climate Model, *J. Adv. Model. Earth Sy.*, 12, e2019MS002010, <https://doi.org/10.1029/2019MS002010>, 2020.
- Brunner, L., Lorenz, R., Zumwald, M., and Knutti, R.: Quantifying uncertainty in European climate projections using combined performance-independence weighting, *Environ. Res. Lett.*, 14, 124010, <https://doi.org/10.1088/1748-9326/ab492f>, 2019.
- Brunner, L., Pendergrass, A. G., Lehner, F., Merrifield, A. L., Lorenz, R., and Knutti, R.: Reduced global warming from CMIP6 projections when weighting models by performance and independence, *Earth Syst. Dynam.*, 11, 995–1012, <https://doi.org/10.5194/esd-11-995-2020>, 2020.
- Cannon, A. J.: Selecting GCM Scenarios that Span the Range of Changes in a Multimodel Ensemble: Application to CMIP5 Climate Extremes Indices, *J. Climate*, 28, 1260–1267, <https://doi.org/10.1175/JCLI-D-14-00636.1>, 2015.
- Cannon, A. J., Sobie, S. R., and Murdock, T. Q.: Bias Correction of GCM Precipitation by Quantile Mapping: How Well Do Methods Preserve Changes in Quantiles and Extremes?, *J. Climate*, 28, 6938–6959, <https://doi.org/10.1175/JCLI-D-14-00754.1>, 2015.
- Cao, J., Wang, B., Yang, Y.-M., Ma, L., Li, J., Sun, B., Bao, Y., He, J., Zhou, X., and Wu, L.: The NUIST Earth System Model (NESM) version 3: description and preliminary evaluation, *Geosci. Model Dev.*, 11, 2975–2993, <https://doi.org/10.5194/gmd-11-2975-2018>, 2018.
- Casanueva, A., Bedia, J., Herrera García, S., Fernández, J., and Gutiérrez, J.: Direct and component-wise bias correction of multi-variate climate indices: the percentile adjustment function diagnostic tool, *Climatic Change*, 147, 411–425, <https://doi.org/10.1007/s10584-018-2167-5>, 2018.
- Casanueva, A., Herrera, S., Iturbide, M., Lange, S., Jury, M., Dosio, A., Maraun, D., and Gutiérrez, J. M.: Testing bias adjustment methods for regional climate change applications under observational uncertainty and resolution mismatch, *Atmos. Sci. Lett.*, 21, e978, <https://doi.org/10.1002/asl.978>, 2020.
- Cheab, A., Badeau, V., Boe, J., Chuine, I., Delire, C., Dufresne, E., François, C., Gritti, E. S., Legay, M., Pagé, C., Thuiller, W., Viomy, N., and Leadley, P.: Climate change impacts on tree ranges: model intercomparison facilitates understanding and quantification of uncertainty, *Ecol. Lett.*, 15, 533–544, <https://doi.org/10.1111/j.1461-0248.2012.01764.x>, 2012.
- Chen, J., Brissette, F. P., and Leconte, R.: Uncertainty of downscaling method in quantifying the impact of climate change on hydrology, *J. Hydrol.*, 401, 190–202, <https://doi.org/10.1016/j.jhydrol.2011.02.020>, 2011.
- Cherchi, A., Fogli, P. G., Lovato, T., Peano, D., Iovino, D., Gualdi, S., Masina, S., Scoccimarro, E., Matera, S., Bellucci, A., and Navarra, A.: Global Mean Climate and Main Patterns of Variability in the CMCC-CM2 Coupled Model, *J. Adv. Model. Earth Sy.*, 11, 185–209, <https://doi.org/10.1029/2018MS001369>, 2019.
- Cleverly, J., Eamus, D., Luo, Q., Restrepo-Coupe, N., Kljun, N., Ma, X., Ewenz, C., Li, L., Yu, Q., and Huete, A.: The importance of interacting climate modes on Australia's contri-

- bution to global carbon cycle extremes, *Sci. Rep.*, 6, 23113, <https://doi.org/10.1038/srep23113>, 2016.
- Deo, R. and Şahin, M.: Application of the extreme learning machine algorithm for the prediction of monthly Effective Drought Index in eastern Australia, *Atmos. Res.*, 153, 512–525, <https://doi.org/10.1016/j.atmosres.2014.10.016>, 2015.
- Déqué, M.: Frequency of precipitation and temperature extremes over France in an anthropogenic scenario: Model results and statistical correction according to observed values, *Global Planet. Change*, 57, 16–26, <https://doi.org/10.1016/j.gloplacha.2006.11.030>, 2007.
- Déqué, M. and Somot, S.: Weighted frequency distributions express modelling uncertainties in the ENSEMBLES regional climate experiments, *Clim. Res.*, 44, 195–209, <https://doi.org/10.3354/cr00866>, 2010.
- Döscher, R., Acosta, M., Alessandri, A., Anthoni, P., Arsouze, T., Bergman, T., Bernardello, R., Boussetta, S., Caron, L.-P., Carver, G., Castrillo, M., Catalano, F., Cvijanovic, I., Davini, P., Dekker, E., Doblas-Reyes, F. J., Docquier, D., Echevarria, P., Fladrich, U., Fuentes-Franco, R., Gröger, M., v. Hardenberg, J., Hieronymus, J., Karami, M. P., Keskinen, J.-P., Koenigk, T., Makkonen, R., Massonnet, F., Ménégoz, M., Miller, P. A., Moreno-Chamarro, E., Nieradzki, L., van Noije, T., Nolan, P., O'Donnell, D., Olinaho, P., van den Oord, G., Ortega, P., Prims, O. T., Ramos, A., Reerink, T., Rousset, C., Ruprich-Robert, Y., Le Sager, P., Schmith, T., Schrödner, R., Serva, F., Sicardi, V., Sloth Madsen, M., Smith, B., Tian, T., Tourigny, E., Uotila, P., Vancoppenolle, M., Wang, S., Wärlind, D., Willén, U., Wyser, K., Yang, S., Yepes-Arbós, X., and Zhang, Q.: The EC-Earth3 Earth system model for the Coupled Model Intercomparison Project 6, *Geosci. Model Dev.*, 15, 2973–3020, <https://doi.org/10.5194/gmd-15-2973-2022>, 2022.
- Dunne, J. P., Horowitz, L. W., Adcroft, A. J., Ginoux, P., Held, I. M., John, J. G., Krasting, J. P., Malyshev, S., Naik, V., Paulot, F., Shevliakova, E., Stock, C. A., Zadeh, N., Balaji, V., Blanton, C., Dunne, K. A., Dupuis, C., Durachta, J., Dussin, R., Gauthier, P. P. G., Griffies, S. M., Guo, H., Hallberg, R. W., Harrison, M., He, J., Hurlin, W., McHugh, C., Menzel, R., Milly, P. C. D., Nikonov, S., Paynter, D. J., Ploshay, J., Radhakrishnan, A., Rand, K., Reichl, B. G., Robinson, T., Schwarzkopf, D. M., Sentman, L. T., Underwood, S., Vahlenkamp, H., Winton, M., Wittenberg, A. T., Wyman, B., Zeng, Y., and Zhao, M.: The GFDL Earth System Model Version 4.1 (GFDL-ESM 4.1): Overall Coupled Model Description and Simulation Characteristics, *J. Adv. Model. Earth Sy.*, 12, e2019MS002015, <https://doi.org/10.1029/2019MS002015>, 2020.
- ESGF: CMIP6 output, <https://esgf-node.llnl.gov/search/cmip6/>, last access: 1 May 2023.
- Evans, J. P., Ji, F., Lee, C., Smith, P., Argüeso, D., and Fita, L.: Design of a regional climate modelling projection ensemble experiment – NARCLiM, *Geosci. Model Dev.*, 7, 621–629, <https://doi.org/10.5194/gmd-7-621-2014>, 2014.
- Famien, A. M., Janicot, S., Ochou, A. D., Vrac, M., Defrance, D., Sultan, B., and Noël, T.: A bias-corrected CMIP5 dataset for Africa using the CDF-t method – a contribution to agricultural impact studies, *Earth Syst. Dynam.*, 9, 313–338, <https://doi.org/10.5194/esd-9-313-2018>, 2018.
- Fisher, R., McDowell, N., Purves, D., Moorcroft, P., Sitch, S., Cox, P., Huntingford, C., Meir, P., and Woodward, I. F.: Assessing uncertainties in a second-generation dynamic vegetation model caused by ecological scale limitations, *New Phytol.*, 187, 666–681, <https://doi.org/10.1111/j.1469-8137.2010.03340.x>, 2010.
- Fisher, R. A., Koven, C. D., Anderegg, W. R. L., Christoffersen, B. O., Dietze, M. C., Farnior, C. E., Holm, J. A., Hurtt, G. C., Knox, R. G., Lawrence, P. J., Lichstein, J. W., Longo, M., Matheny, A. M., Medvigy, D., Muller-Landau, H. C., Powell, T. L., Serbin, S., Sato, H., Shuman, J. K., Smith, B., Trugman, A. T., Viskari, T., Verbeeck, H., Weng, E., Xu, C., Xu, X., Zhang, T., and Moorcroft, P. R.: Vegetation demographics in Earth System Models: A review of progress and priorities, *Glob. Change Biol.*, 24, 35–54, <https://doi.org/10.1111/gcb.13910>, 2018.
- Flato, G., Marotzke, J., Abiodun, B., Braconnot, P., Chou, S. C., Collins, W., Cox, P., Driouech, F., Emori, S., Eyring, V., Forest, C., Gleckler, P., Guilyardi, E., Jakob, C., Kattsov, V., Reason, C., and Rummukainen, M.: Evaluation of climate models, in: *Climate Change 2013: The Physical Science Basis. Contribution of Working Group I to the Fifth Assessment Report of the Intergovernmental Panel on Climate Change*, edited by: Stocker, T. F., Qin, D., Plattner, G.-K., Tignor, M., Allen, S. K., Doschung, J., Nauels, A., Xia, Y., Bex, V., and Midgley, P. M., 741–882, Cambridge University Press, Cambridge, UK, <https://doi.org/10.1017/CBO9781107415324.020>, 2013.
- François, B., Vrac, M., Cannon, A. J., Robin, Y., and Allard, D.: Multivariate bias corrections of climate simulations: which benefits for which losses?, *Earth Syst. Dynam.*, 11, 537–562, <https://doi.org/10.5194/esd-11-537-2020>, 2020.
- Freedman, D. and Diaconis, P.: On the histogram as a density estimator: L2 theory, *Z. Wahrscheinlichkeit.*, 57, 453–476, 1981.
- Gallagher, R. V., Butt, N., Carthey, A. J. R., Tulloch, A., Bland, L., Clulow, S., Newsome, T., Dudanec, R. Y., and Adams, V. M.: A guide to using species trait data in conservation, *One Earth*, 4, 927–936, <https://doi.org/10.1016/j.oneear.2021.06.013>, 2021.
- Gershunov, A., Shulgina, T., Clemesha, R., Guirguis, K., Pierce, D., Dettinger, M., Lavers, D., Cayan, D., Polade, S., Kalansky, J., and Ralph, F.: Precipitation regime change in Western North America: The role of Atmospheric Rivers, *Sci. Rep.*, 9, 9944, <https://doi.org/10.1038/s41598-019-46169-w>, 2019.
- Gohar, L. K., Lowe, J. A., and Bernie, D.: The Impact of Bias Correction and Model Selection on Passing Temperature Thresholds, *J. Geophys. Res.-Atmos.*, 122, 12045–12061, <https://doi.org/10.1002/2017JD026797>, 2017.
- Grose, M. R., Narsey, S., Delage, F. P., Dowdy, A. J., Bador, M., Boschat, G., Chung, C., Kajtar, J. B., Rauniyar, S., Freund, M. B., Lyu, K., Rashid, H., Zhang, X., Wales, S., Trenham, C., Holbrook, N. J., Cowan, T., Alexander, L., Arblaster, J. M., and Power, S.: Insights From CMIP6 for Australia's Future Climate, *Earth's Future*, 8, e2019EF001469, <https://doi.org/10.1029/2019EF001469>, 2020.
- Hagemann, S., Chen, C., Haerter, J. O., Heinke, J., Gerten, D., and Piani, C.: Impact of a Statistical Bias Correction on the Projected Hydrological Changes Obtained from Three GCMs and Two Hydrology Models, *J. Hydrometeorol.*, 12, 556–578, <https://doi.org/10.1175/2011JHM1336.1>, 2011.
- Harris, I.: CRU JRA v2.0: A forcings dataset of gridded land surface blend of Climatic Research Unit (CRU) and Japanese reanalysis (JRA) data; Jan.1901–Dec.2018, Centre for Environmental Data Analysis (CEDA) [data set], <https://catalogue>.



- ceda.ac.uk/uuid/7f785c0e80aa4df2b39d068ce7351bbb (last access: March 2021), 2019.
- Harris, I., Jones, P., Osborn, T., and Lister, D.: Updated high-resolution grids of monthly climatic observations – the CRU TS3.10 Dataset, *Int. J. Climatol.*, 34, 623–642, <https://doi.org/10.1002/joc.3711>, 2014.
- Haughton, N., Abramowitz, G., and Pitman, A. J.: On the predictability of land surface fluxes from meteorological variables, *Geosci. Model Dev.*, 11, 195–212, <https://doi.org/10.5194/gmd-11-195-2018>, 2018.
- Haverd, V., Raupach, M. R., Briggs, P. R., Canadell, J. G., Davis, S. J., Law, R. M., Meyer, C. P., Peters, G. P., Pickett-Heaps, C., and Sherman, B.: The Australian terrestrial carbon budget, *Biogeosciences*, 10, 851–869, <https://doi.org/10.5194/bg-10-851-2013>, 2013.
- Held, I. M., Guo, H., Adcroft, A., Dunne, J. P., Horowitz, L. W., Krasting, J., Shevliakova, E., Winton, M., Zhao, M., Bushuk, M., Wittenberg, A. T., Wyman, B., Xiang, B., Zhang, R., Anderson, W., Balaji, V., Donner, L., Dunne, K., Durachta, J., Gauthier, P. P. G., Ginoux, P., Golaz, J.-C., Griffies, S. M., Hallberg, R., Harris, L., Harrison, M., Hurlin, W., John, J., Lin, P., Lin, S.-J., Malyshev, S., Menzel, R., Milly, P. C. D., Ming, Y., Naik, V., Paynter, D., Paulot, F., Ramaswamy, V., Reichl, B., Robinson, T., Rosati, A., Seman, C., Silvers, L. G., Underwood, S., and Zadeh, N.: Structure and Performance of GFDL's CM4.0 Climate Model, *J. Adv. Model. Earth Sy.*, 11, 3691–3727, <https://doi.org/10.1029/2019MS001829>, 2019.
- Heger, N., Abramowitz, G., Knutti, R., Angéllil, O., Lehmann, K., and Sanderson, B. M.: Selecting a climate model subset to optimise key ensemble properties, *Earth Syst. Dynam.*, 9, 135–151, <https://doi.org/10.5194/esd-9-135-2018>, 2018.
- Heger, N., Abramowitz, G., Sherwood, S., Knutti, R., Angéllil, O., and Sisson, S.: Ensemble optimisation, multiple constraints and overconfidence: a case study with future Australian precipitation change, *Clim. Dynam.*, 53, 1581–1596, <https://doi.org/10.1007/s00382-019-04690-8>, 2019.
- Hersbach, H., Bell, B., Berrisford, P., Hirahara, S., Horányi, A., Muñoz-Sabater, J., Nicolas, J., Peubey, C., Radu, R., Schepers, D., Simmons, A., Soci, C., Abdalla, S., Abellan, X., Balsamo, G., Bechtold, P., Biavati, G., Bidlot, J., Bonavita, M., De Chiara, G., Dahlgren, P., Dee, D., Diamantakis, M., Dragani, R., Fleming, J., Forbes, R., Fuentes, M., Geer, A., Haimberger, L., Healy, S., Hogan, R. J., Hólm, E., Janisková, M., Keeley, S., Laloyaux, P., Lopez, P., Lupu, C., Radnoti, G., de Rosnay, P., Rozum, I., Vamborg, F., Villaume, S., and Thépaut, J.-N.: The ERA5 global reanalysis, *Q. J. Roy. Meteor. Soc.*, 146, 1999–2049, <https://doi.org/10.1002/qj.3803>, 2020.
- Huntingford, C., Jeffers, E. S., Bonsall, M. B., Christensen, H. M., Lees, T., and Yang, H.: Machine learning and artificial intelligence to aid climate change research and preparedness, *Environ. Res. Lett.*, 14, 124007, <https://doi.org/10.1088/1748-9326/ab4e55>, 2019.
- Iizumi, T., Takikawa, H., Hirabayashi, Y., Hanasaki, N., and Nishimori, M.: Contributions of different bias-correction methods and reference meteorological forcing data sets to uncertainty in projected temperature and precipitation extremes, *J. Geophys. Res.-Atmos.*, 122, 7800–7819, <https://doi.org/10.1002/2017JD026613>, 2017.
- IPCC: Climate Change 2013: The Physical Science Basis. Contribution of Working Group I to the Fifth Assessment Report of the Intergovernmental Panel on Climate Change, edited by: Stocker, T., Qin, D., Plattner, G.-K., Tignor, M., Allen, S., Boschung, J., Nauels, A., Xia, Y., Bex, V., and Midgley, P. M., Cambridge University Press, Cambridge, United Kingdom and New York, NY, USA, <https://doi.org/10.1017/CBO9781107415324>, 2013.
- IPCC: Regional fact sheet – Australasia, in: Climate Change 2021: The Physical Science Basis. Contribution of Working Group I to the Sixth Assessment Report of the Intergovernmental Panel on Climate Change, edited by: Masson-Delmotte, V., Zhai, P., Pirani, A., Connors, S. L., Péan, C., Berger, S., Caud, N., Chen, Y., Goldfarb, L., Gomis, M. I., Huang, M., Leitzell, K., Lonnoy, E., Matthews, J., Maycock, T., Waterfield, T., Yelekçi, O., Yu, R., and Zhou, B., Cambridge University Press, Cambridge, United Kingdom and New York, NY, USA, 2021.
- Johnson, F. and Sharma, A.: What are the impacts of bias correction on future drought projections?, *J. Hydrol.*, 525, 472–485, <https://doi.org/10.1016/j.jhydrol.2015.04.002>, 2015.
- Jun, M., Knutti, R., and Nychka, D. W.: Spatial Analysis to Quantify Numerical Model Bias and Dependence, *J. Am. Stat. Assoc.*, 103, 934–947, <https://doi.org/10.1198/016214507000001265>, 2008.
- Jung, M., Reichstein, M., Ciais, P., Seneviratne, S., Sheffield, J., Goulden, M., Bonan, G., Cescatti, A., Chen, J., de Jeu, R., Dolman, H. A., Eugster, W., Gerten, D., Gianelle, D., Gobron, N., Heinke, J., Kimball, J., Law, B., and Montagnani, L.: Recent Decline in the Global Land Evapotranspiration Trend Due to Limited Moisture Supply, *Nature*, 467, 951–954, <https://doi.org/10.1038/nature09396>, 2010.
- Knutti, R., Abramowitz, G., Collins, M., Eyring, V., Gleckler, P., Hewitson, B., and Mearns, L.: Good Practice Guidance Paper on Assessing and Combining Multi Model Climate Projections, Meeting Report of the Intergovernmental Panel on Climate Change Expert Meeting on Assessing and Combining Multi Model Climate Projections, edited by: Stocker, T. F., Qin, D., Plattner, G.-K., Tignor, M., and Midgley, P. M., IPCC Working Group I Technical Support Unit, University of Bern, 582 pp., 2010a.
- Knutti, R., Furrer, R., Tebaldi, C., Cermak, J., and Meehl, G. A.: Challenges in Combining Projections from Multiple Climate Models, *J. Climate*, 23, 2739–2758, <https://doi.org/10.1175/2009JCLI3361.1>, 2010b.
- Knutti, R., Sedláček, J., Sanderson, B. M., Lorenz, R., Fischer, E. M., and Eyring, V.: A climate model projection weighting scheme accounting for performance and interdependence, *Geophys. Res. Lett.*, 44, 1909–1918, <https://doi.org/10.1002/2016GL072012>, 2017.
- Kobayashi, S., Ota, Y., Harada, Y., Ebata, A., Moriya, M., Onoda, H., Onogi, K., Kamahori, H., Kobayashi, C., Endo, H., Miyaoka, K., and Takahashi, K.: The JRA-55 Reanalysis: General Specifications and Basic Characteristics, *J. Meteorol. Soc. Jpn. Ser. II*, 93, 5–48, <https://doi.org/10.2151/jmsj.2015-001>, 2015.
- Kolusu, S. R., Siderius, C., Todd, M. C., Bhave, A., Conway, D., James, R., Washington, R., Geressu, R., Harou, J. J., and Kashaigili, J. J.: Sensitivity of projected climate impacts to climate model weighting: multi-sector analysis in eastern Africa, *Climatic Change*, 164, 36, <https://doi.org/10.1007/s10584-021-02991-8>, 2021.

- Lamarque, J.-F., Dentener, F., McConnell, J., Ro, C.-U., Shaw, M., Vet, R., Bergmann, D., Cameron-Smith, P., Dalsoren, S., Doherty, R., Faluvegi, G., Ghan, S. J., Josse, B., Lee, Y. H., MacKenzie, I. A., Plummer, D., Shindell, D. T., Skeie, R. B., Stevenson, D. S., Strode, S., Zeng, G., Curran, M., Dahl-Jensen, D., Das, S., Fritzsche, D., and Nolan, M.: Multi-model mean nitrogen and sulfur deposition from the Atmospheric Chemistry and Climate Model Intercomparison Project (ACCMIP): evaluation of historical and projected future changes, *Atmos. Chem. Phys.*, 13, 7997–8018, <https://doi.org/10.5194/acp-13-7997-2013>, 2013.
- Law, R. M., Ziehn, T., Matear, R. J., Lenton, A., Chamberlain, M. A., Stevens, L. E., Wang, Y.-P., Srbinovsky, J., Bi, D., Yan, H., and Vohralik, P. F.: The carbon cycle in the Australian Community Climate and Earth System Simulator (ACCESS-ESM1) – Part I: Model description and pre-industrial simulation, *Geosci. Model Dev.*, 10, 2567–2590, <https://doi.org/10.5194/gmd-10-2567-2017>, 2017.
- Liu, S.-M., Chen, Y.-H., Rao, J., Cao, C., Li, S.-Y., Ma, M.-H., and Wang, Y.-B.: Parallel Comparison of Major Sudden Stratospheric Warming Events in CESM1-WACCM and CESM2-WACCM, *Atmosphere*, 10, 679, <https://doi.org/10.3390/atmos10110679>, 2019.
- Liu, Y., Racah, E., Prabhat, Correa, J., Khosrowshahi, A., Lavers, D., Kunkel, K., Wehner, M., and Collins, W.: Application of Deep Convolutional Neural Networks for Detecting Extreme Weather in Climate Datasets, *arXiv [preprint]*, <https://doi.org/10.48550/arXiv.1605.01156>, 4 May 2016.
- Maraun, D., Shepherd, T., Widmann, M., Zappa, G., Walton, D., Gutiérrez, J., Hagemann, S., Richter, I., Soares, P., Hall, A., and Mearns, L.: Towards process-informed bias correction of climate change simulations, *Nat. Clim. Change*, 7, 3418, <https://doi.org/10.1038/nclimate3418>, 2017.
- Martyn Clark, M., Gangopadhyay, S., Hay, L., Rajagopalan, B., and Wilby, R.: The Schaake Shuffle: A Method for Reconstructing Space–Time Variability in Forecasted Precipitation and Temperature Fields, *J. Hydrometeorol.*, 5, 243–262, [https://doi.org/10.1175/1525-7541\(2004\)005<0243:TSSAMF>2.0.CO;2](https://doi.org/10.1175/1525-7541(2004)005<0243:TSSAMF>2.0.CO;2), 2004.
- Massoud, E., Espinoza, V., Guan, B., and Waliser, D.: Global Climate Model Ensemble Approaches for Future Projections of Atmospheric Rivers, *Earth's Future*, 7, 1136–1151, <https://doi.org/10.1029/2019EF001249>, 2019.
- Massoud, E. C., Lee, H., Gibson, P. B., Loikith, P., and Waliser, D. E.: Bayesian Model Averaging of Climate Model Projections Constrained by Precipitation Observations over the Contiguous United States, *J. Hydrometeorol.*, 21, 2401–2418, <https://doi.org/10.1175/JHM-D-19-0258.1>, 2020.
- Maurer, E. P. and Pierce, D. W.: Bias correction can modify climate model simulated precipitation changes without adverse effect on the ensemble mean, *Hydrol. Earth Syst. Sci.*, 18, 915–925, <https://doi.org/10.5194/hess-18-915-2014>, 2014.
- Mauritsen, T., Bader, J., Becker, T., Behrens, J., Bittner, M., Brokopf, R., Brovkin, V., Claussen, M., Crueger, T., Esch, M., Fast, I., Fiedler, S., Fläschner, D., Gayler, V., Giorgetta, M., Goll, D. S., Haak, H., Hagemann, S., Hedemann, C., Hohenegger, C., Ilyina, T., Jahns, T., Jimenéz-de-la Cuesta, D., Jungclaus, J., Kleinen, T., Kloster, S., Kracher, D., Kinne, S., Kleberg, D., Lasslop, G., Kornblüeh, L., Marotzke, J., Matei, D., Meraner, K., Mikolajewicz, U., Modali, K., Möbis, B., Müller, W. A., Nabel, J. E. M. S., Nam, C. C. W., Notz, D., Nyawira, S.-S., Paulsen, H., Peters, K., Pincus, R., Pohlmann, H., Pongratz, J., Popp, M., Raddatz, T. J., Rast, S., Redler, R., Reick, C. H., Rohrschneider, T., Schemann, V., Schmidt, H., Schnur, R., Schulzweida, U., Six, K. D., Stein, L., Stemmler, I., Stevens, B., von Storch, J.-S., Tian, F., Voigt, A., Vrese, P., Wieners, K.-H., Wilkenskjaeld, S., Winkler, A., and Roeckner, E.: Developments in the MPI-M Earth System Model version 1.2 (MPI-ESM1.2) and Its Response to Increasing CO<sub>2</sub>, *J. Adv. Model. Earth Sy.*, 11, 998–1038, <https://doi.org/10.1029/2018MS001400>, 2019.
- Meinshausen, M., Nicholls, Z. R. J., Lewis, J., Gidden, M. J., Vogel, E., Freund, M., Beyerle, U., Gessner, C., Nauels, A., Bauer, N., Canadell, J. G., Daniel, J. S., John, A., Krummel, P. B., Luderer, G., Meinshausen, N., Montzka, S. A., Rayner, P. J., Reimann, S., Smith, S. J., van den Berg, M., Velders, G. J. M., Vollmer, M. K., and Wang, R. H. J.: The shared socio-economic pathway (SSP) greenhouse gas concentrations and their extensions to 2500, *Geosci. Model Dev.*, 13, 3571–3605, <https://doi.org/10.5194/gmd-13-3571-2020>, 2020.
- Merrifield, A. L., Brunner, L., Lorenz, R., Medhaug, I., and Knutti, R.: An investigation of weighting schemes suitable for incorporating large ensembles into multi-model ensembles, *Earth Syst. Dynam.*, 11, 807–834, <https://doi.org/10.5194/esd-11-807-2020>, 2020.
- Michelangeli, P.-A., Vrac, M., and Loukos, H.: Probabilistic downscaling approaches: Application to wind cumulative distribution functions, *Geophys. Res. Lett.*, 36, L11708, <https://doi.org/10.1029/2009GL038401>, 2009.
- Müller, W. A., Jungclaus, J. H., Mauritsen, T., Baehr, J., Bittner, M., Budich, R., Bunzel, F., Esch, M., Ghosh, R., Haak, H., Ilyina, T., Kleine, T., Kornblüeh, L., Li, H., Modali, K., Notz, D., Pohlmann, H., Roeckner, E., Stemmler, I., Tian, F., and Marotzke, J.: A Higher-resolution Version of the Max Planck Institute Earth System Model (MPI-ESM1.2-HR), *J. Adv. Model. Earth Sy.*, 10, 1383–1413, <https://doi.org/10.1029/2017MS001217>, 2018.
- Pak, G., Noh, Y., Lee, M.-I., Yeh, S.-W., Kim, D., Kim, S.-Y., Lee, J.-L., Lee, H., Hyun, S.-H., Lee, K.-Y., Lee, J.-H., Park, Y.-G., Jin, H., Park, H., and Kim, Y.: Korea Institute of Ocean Science and Technology Earth System Model and Its Simulation Characteristics, *Ocean Sci. J.*, 56, 18–45, <https://doi.org/10.1007/s12601-021-00001-7>, 2021.
- Panofsky, H. A., Brier, G. W., and Best, W. H.: Some application of statistics to meteorology, 1958.
- Pennell, C. and Reichler, T.: On the Effective Number of Climate Models, *J. Climate*, 24, 2358–2367, <https://doi.org/10.1175/2010JCLI3814.1>, 2011.
- Pierce, D., Barnett, T., Santer, B., and Gleckler, P.: Selecting Global Climate Models for Regional Climate Change Studies, *P. Natl. Acad. Sci. USA*, 106, 8441–8446, <https://doi.org/10.1073/pnas.0900094106>, 2009.
- Poulter, B., Frank, D., Ciais, P., Myneni, R., Andela, N., Bi, J., Broquet, G., Canadell, J., Chevallier, F., Liu, Y., Running, S., Sitch, S., and van der Werf, G.: Contribution of semi-arid ecosystems to interannual variability of the global carbon cycle, *Nature*, 509, 600–603, <https://doi.org/10.1038/nature13376>, 2014.
- Randall, D. A., Wood, R. A., Bony, S., Colman, R., Fichet, T., Fyfe, J., Kattsov, V., Pitman, A., Shukla, J., Srinivasan, J., Stouf-

- fer, R. J., Sumi, A., and Taylor, K. E.: Climate models and their evaluation, Chap. 8, in: *Climate Change 2007: the physical science basis. Contribution of Working Group I to the Fourth Assessment Report of the Intergovernmental Panel on Climate Change*, edited by: Solomon, S., Qin, D., Manning, M., Chen, Z., Marquis, M., Averyt, K. B., Tignor, M., and Miller, H. L., 589–662, Cambridge University Press, Cambridge, UK, 2007.
- Robin, Y.: SBCK (Statistical Bias Correction Kit), GitHub [code], <https://github.com/yrobink/SBCK>, last access: 1 July 2022.
- Robin, Y. and Vrac, M.: Is time a variable like the others in multivariate statistical downscaling and bias correction?, *Earth Syst. Dynam.*, 12, 1253–1273, <https://doi.org/10.5194/esd-12-1253-2021>, 2021.
- Robin, Y., Vrac, M., Naveau, P., and Yiou, P.: Multivariate stochastic bias corrections with optimal transport, *Hydrol. Earth Syst. Sci.*, 23, 773–786, <https://doi.org/10.5194/hess-23-773-2019>, 2019.
- Rowell, D. P., Senior, C. A., Vellinga, M. L., and Graham, R. J.: Can climate projection uncertainty be constrained over Africa using metrics of contemporary performance?, *Climatic Change*, 134, 621–633, 2016.
- Sanderson, B. M., Wehner, M., and Knutti, R.: Skill and independence weighting for multi-model assessments, *Geosci. Model Dev.*, 10, 2379–2395, <https://doi.org/10.5194/gmd-10-2379-2017>, 2017.
- Seland, Ø., Bentsen, M., Olivie, D., Toniazzo, T., Gjermundsen, A., Graff, L. S., Debernard, J. B., Gupta, A. K., He, Y.-C., Kirkevåg, A., Schwinger, J., Tjiputra, J., Aas, K. S., Bethke, L., Fan, Y., Griesfeller, J., Grini, A., Guo, C., Ilicak, M., Karset, I. H. H., Landgren, O., Liakka, J., Moseid, K. O., Nummelin, A., Spensberger, C., Tang, H., Zhang, Z., Heinze, C., Iversen, T., and Schulz, M.: Overview of the Norwegian Earth System Model (NorESM2) and key climate response of CMIP6 DECK, historical, and scenario simulations, *Geosci. Model Dev.*, 13, 6165–6200, <https://doi.org/10.5194/gmd-13-6165-2020>, 2020.
- Sitch, S., Smith, B., Prentice, I. C., Arneth, A., Bondeau, A., Cramer, W., Kaplan, J. O., Levis, S., Lucht, W., Sykes, M. T., Thonicke, K., and Venevsky, S.: Evaluation of ecosystem dynamics, plant geography and terrestrial carbon cycling in the LPJ dynamic global vegetation model, *Glob. Change Biol.*, 9, 161–185, <https://doi.org/10.1046/j.1365-2486.2003.00569.x>, 2003.
- Smith, B., Wårlind, D., Arneth, A., Hickler, T., Leadley, P., Siltberg, J., and Zaehle, S.: Implications of incorporating N cycling and N limitations on primary production in an individual-based dynamic vegetation model, *Biogeosciences*, 11, 2027–2054, <https://doi.org/10.5194/bg-11-2027-2014>, 2014.
- Sperry, J. S., Venturas, M. D., Todd, H. N., Trugman, A. T., Anderegg, W. R. L., Wang, Y., and Tai, X.: The impact of rising CO<sub>2</sub> and acclimation on the response of US forests to global warming, *P. Natl. Acad. Sci. USA*, 116, 25734–25744, <https://doi.org/10.1073/pnas.1913072116>, 2019.
- Swart, N. C., Cole, J. N. S., Kharin, V. V., Lazare, M., Scinocca, J. F., Gillett, N. P., Anstey, J., Arora, V., Christian, J. R., Hanna, S., Jiao, Y., Lee, W. G., Majaess, F., Saenko, O. A., Seiler, C., Seinen, C., Shao, A., Sigmund, M., Solheim, L., von Salzen, K., Yang, D., and Winter, B.: The Canadian Earth System Model version 5 (CanESM5.0.3), *Geosci. Model Dev.*, 12, 4823–4873, <https://doi.org/10.5194/gmd-12-4823-2019>, 2019.
- Tatebe, H., Ogura, T., Nitta, T., Komuro, Y., Ogochi, K., Takemura, T., Sudo, K., Sekiguchi, M., Abe, M., Saito, F., Chikira, M., Watanabe, S., Mori, M., Hirota, N., Kawatani, Y., Mochizuki, T., Yoshimura, K., Takata, K., O'ishi, R., Yamazaki, D., Suzuki, T., Kurogi, M., Kataoka, T., Watanabe, M., and Kimoto, M.: Description and basic evaluation of simulated mean state, internal variability, and climate sensitivity in MIROC6, *Geosci. Model Dev.*, 12, 2727–2765, <https://doi.org/10.5194/gmd-12-2727-2019>, 2019.
- Teckentrup, L.: lteckentrup/CMIP6\_australia: Analysis code submission (v1.0.0), Zenodo [code], <https://doi.org/10.5281/zenodo.7882380>, 2023.
- Teckentrup, L., De Kauwe, M. G., Pitman, A. J., Goll, D. S., Haverd, V., Jain, A. K., Joetjzer, E., Kato, E., Lienert, S., Lombardozzi, D., McGuire, P. C., Melton, J. R., Nabel, J. E. M. S., Pongratz, J., Sitch, S., Walker, A. P., and Zaehle, S.: Assessing the representation of the Australian carbon cycle in global vegetation models, *Biogeosciences*, 18, 5639–5668, <https://doi.org/10.5194/bg-18-5639-2021>, 2021.
- Thao, S., Garvik, M., Mariethoz, G., and Vrac, M.: Combining global climate models using graph cuts, *Clim. Dynam.*, 59, 2345–2361, <https://doi.org/10.1007/s00382-022-06213-4>, 2022.
- Thonicke, K., Venevsky, S., Sitch, S., and Cramer, W.: The role of fire disturbance for global vegetation dynamics: Coupling fire into a Dynamic Global Vegetation Model, *Global Ecol. Biogeogr.*, 10, 661–677, <https://doi.org/10.1046/j.1466-822X.2001.00175.x>, 2001.
- Ukkola, A. M., Keenan, T. F., Kelley, D. I., and Prentice, I. C.: Vegetation plays an important role in mediating future water resources, *Environ. Res. Lett.*, 11, 094022, <https://doi.org/10.1088/1748-9326/11/9/094022>, 2016.
- Ukkola, A. M., De Kauwe, M. G., Roderick, M. L., Abramowitz, G., and Pitman, A. J.: Robust Future Changes in Meteorological Drought in CMIP6 Projections Despite Uncertainty in Precipitation, *Geophys. Res. Lett.*, 47, e2020GL087820, <https://doi.org/10.1029/2020GL087820>, 2020.
- Volodin, E. M., Mortikov, E. V., Kostykin, S. V., Galin, V. Y., Lykossov, V. N., Gritsun, A. S., Nikolay A. Diansky, N. A., Gusev, A. V., Iakovlev, N. G., Shestakova, A. A., and Emelina, S. V.: Simulation of the modern climate using the INM-CM48 climate model, *Russ J. Numer. Anal. M.*, 33, 367–374, <https://doi.org/10.1515/rnam-2018-0032>, 2018.
- Vrac, M.: Multivariate bias adjustment of high-dimensional climate simulations: the Rank Resampling for Distributions and Dependences (R2D2) bias correction, *Hydrol. Earth Syst. Sci.*, 22, 3175–3196, <https://doi.org/10.5194/hess-22-3175-2018>, 2018.
- Vrac, M., Drobinski, P., Merlo, A., Herrmann, M., Lavaysse, C., Li, L., and Somot, S.: Dynamical and statistical downscaling of the French Mediterranean climate: uncertainty assessment, *Nat. Hazards Earth Syst. Sci.*, 12, 2769–2784, <https://doi.org/10.5194/nhess-12-2769-2012>, 2012.
- Wang, B., Zheng, L., Liu, D. L., Ji, F., Clark, A., and Yu, Q.: Using multi-model ensembles of CMIP5 global climate models to reproduce observed monthly rainfall and temperature with machine learning methods in Australia, *Int. J. Climatol.*, 38, 4891–4902, <https://doi.org/10.1002/joc.5705>, 2018.
- Wood, A., Leung, L., Sridhar, V., and Lettenmaier, D.: Hydrologic Implications of Dynamical and Statistical Approaches to Down-

- scaling Climate Model Outputs, *Climatic Change*, 62, 189–216, <https://doi.org/10.1023/B:CLIM.0000013685.99609.9e>, 2004.
- Wu, C., Chen, Y., Peng, C., Li, Z., and Hong, X.: Modeling and estimating aboveground biomass of *Dacrydium pierrei* in China using machine learning with climate change, *J. Environ. Manage.*, 234, 167–179, <https://doi.org/10.1016/j.jenvman.2018.12.090>, 2019.
- Wu, T., Lu, Y., Fang, Y., Xin, X., Li, L., Li, W., Jie, W., Zhang, J., Liu, Y., Zhang, L., Zhang, F., Zhang, Y., Wu, F., Li, J., Chu, M., Wang, Z., Shi, X., Liu, X., Wei, M., Huang, A., Zhang, Y., and Liu, X.: The Beijing Climate Center Climate System Model (BCC-CSM): the main progress from CMIP5 to CMIP6, *Geosci. Model Dev.*, 12, 1573–1600, <https://doi.org/10.5194/gmd-12-1573-2019>, 2019.
- Wu, Z., Ahlström, A., Smith, B., Ardö, J., Eklundh, L., Fensholt, R., and Lehsten, V.: Climate data induced uncertainty in model-based estimations of terrestrial primary productivity, *Environ. Res. Lett.*, 12, 064013, <https://doi.org/10.1088/1748-9326/aa6fd8>, 2017.
- Yang, W., Gardelin, M., Olsson, J., and Bosshard, T.: Multi-variable bias correction: application of forest fire risk in present and future climate in Sweden, *Nat. Hazards Earth Syst. Sci.*, 15, 2037–2057, <https://doi.org/10.5194/nhess-15-2037-2015>, 2015.
- Yang, Y., Guan, H., Batelaan, O., McVicar, T., Long, D., Piao, S., Liang, W., Liu, B., Jin, Z., and Simmons, C.: Contrasting response of water use efficiency to drought across global terrestrial ecosystems, *Sci. Rep.*, 6, 23284, <https://doi.org/10.1038/srep23284>, 2016.
- Yukimoto, S., Kawai, H., Koshiro, T., Oshima, N., Yoshida, K., Urakawa, S., Tsujino, H., Deushi, M., Tanaka, T., Hosaka, M., Yabu, S., Yoshimura, H., Shindo, E., Mizuta, R., Obata, A., Adachi, Y., and Ishii, M.: The Meteorological Research Institute Earth System Model Version 2.0, MRI-ESM2.0: Description and Basic Evaluation of the Physical Component, *J. Meteorol. Soc. Jpn. Ser. II*, 97, 931–965, <https://doi.org/10.2151/jmsj.2019-051>, 2019.
- Zscheischler, J., Fischer, E. M., and Lange, S.: The effect of univariate bias adjustment on multivariate hazard estimates, *Earth Syst. Dynam.*, 10, 31–43, <https://doi.org/10.5194/esd-10-31-2019>, 2019.